2016

Regulation of the Anaphase-Promoting Complex Examined at the Single Cell Level

Andrej Ondracka

REGULATION OF THE ANAPHASE-PROMOTING COMPLEX EXAMINED AT THE SINGLE CELL LEVEL

A Thesis Presented to the Faculty of

The Rockefeller University

in Partial Fulfillment of the Requirements for

the degree of Doctor of Philosophy

by

Andrej Ondracka

June 2016

REGULATION OF THE ANAPHASE-PROMOTING COMPLEX EXAMINED AT THE SINGLE CELL LEVEL

Andrej Ondracka, Ph.D.

The Rockefeller University 2016

Cell cycle transitions are driven by oscillations of cyclin-cyclin dependent kinase (CDK) activity and associated cyclin degradation, mediated by ubiquitylation by the anaphase-promoting complex (APC). In this work, I analyzed the regulation of the APC by its activator Cdh1 in budding yeast in single cells. Inactivation of APC-Cdh1 is an important regulatory transition leading to mitotic entry. I developed and characterized a fluorescent biosensor to measure the dynamics of APC-Cdh1 activity in single cells by quantitative time-lapse microscopy. I found that APC-Cdh1 is inactivated with very reliable timing, in contrast with other cell cycle events that occur with considerable variability in timing. The activity of APC-Cdh1 is restrained by multisite phosphorylation by early cyclin-CDKs. Complete removal of phosphorylation control of Cdh1 results in cell cycle arrest before mitotic entry, because persistent APC-Cdh1 activity prevents mitotic cyclin gene expression and accumulation of mitotic cyclins. I show that partial phosphorylation of Cdh1 allows for partial inactivation of APC-Cdh1. Interestingly, incompletely restrained APC-Cdh1 activity causes a variable phenotype in cell cycle progression on the single cell level. This partially penetrant phenotype, caused by incomplete inactivation of APC-Cdh1, is highly complex; even though

some of the cells arrest in the cell cycle, they occasionally complete later cell cycle events with delay and in incorrect order. I show that Cdh1 can be phosphorylated by multiple cyclin-CDKs, and that additional mechanisms of APC-Cdh1 inactivation besides phosphorylation also contribute to robust inactivation. In the last part of the thesis, I examine the global cell cycle-associated transcriptional program and its regulation by cyclin-dependent kinase activity.

Acknowledgments

I wish to thank people who have contributed to this project. First, I wish to thank Fred Cross, my graduate advisor, for giving me the opportunity to carry out my PhD research in his lab, his support and guidance throughout this project. I wish to thank all the Cross lab members, past and present, for a great atmosphere in the lab. In particular, my thanks go to Lu Bai, for guidance through the initial part of my PhD and especially for help with quantitative microscopy; Craig Atkins, Frej Tulin and Jamal Rahi for many fruitful discussions; and Kresti Pecani for excellent technical support. I would also like to thank Larry Sirovich for introducing me to the PCA method for analyzing yeast gene expression datasets. Finally, my thanks go to my friends and family for their support and encouragement.

Table of Contents

List of Figures

List of Tables

Chapter 1: Introduction

1.1. Regulation of the eukaryotic cell cycle by cyclin-dependent kinases and the anaphase-promoting complex

The main driver of cell cycle progression is periodic activity of cyclin-dependent kinases (CDKs) (Morgan, 2007). CDK activity is dependent on its binding partners, cyclins. Periodic CDK activity is achieved by regulated expression and degradation of cyclins (Murray, 2004).

In budding yeast Saccharomyces cerevisiae, a well-studied unicellular eukaryote, a single CDK, named Cdc28, is involved in cell cycle regulation, and is activated at different cell cycle stages by different cyclins. These cyclin-CDK complexes promote the events of G1, S-phase and mitosis (figure 1.1) New cells are born with low CDK activity. Later in the G1, the commitment point, called Start in budding yeast, signals the decision to commit to a new cell cycle, and is marked by expression of G1 cyclins Cln1 and 2 (Cross and Tinkelenberg, 1991; Dirick and Nasmyth, 1991; Richardson et al, 1989; Skotheim et al, 2008). A third G1 cyclin, Cln3, is present already earlier and has a role in sensing cell size (Richardson et al, 1989; Wang et al, 2009). Cln-CDK activity promotes irreversible passage through START and promotes bud emergence. Cln-CDKs

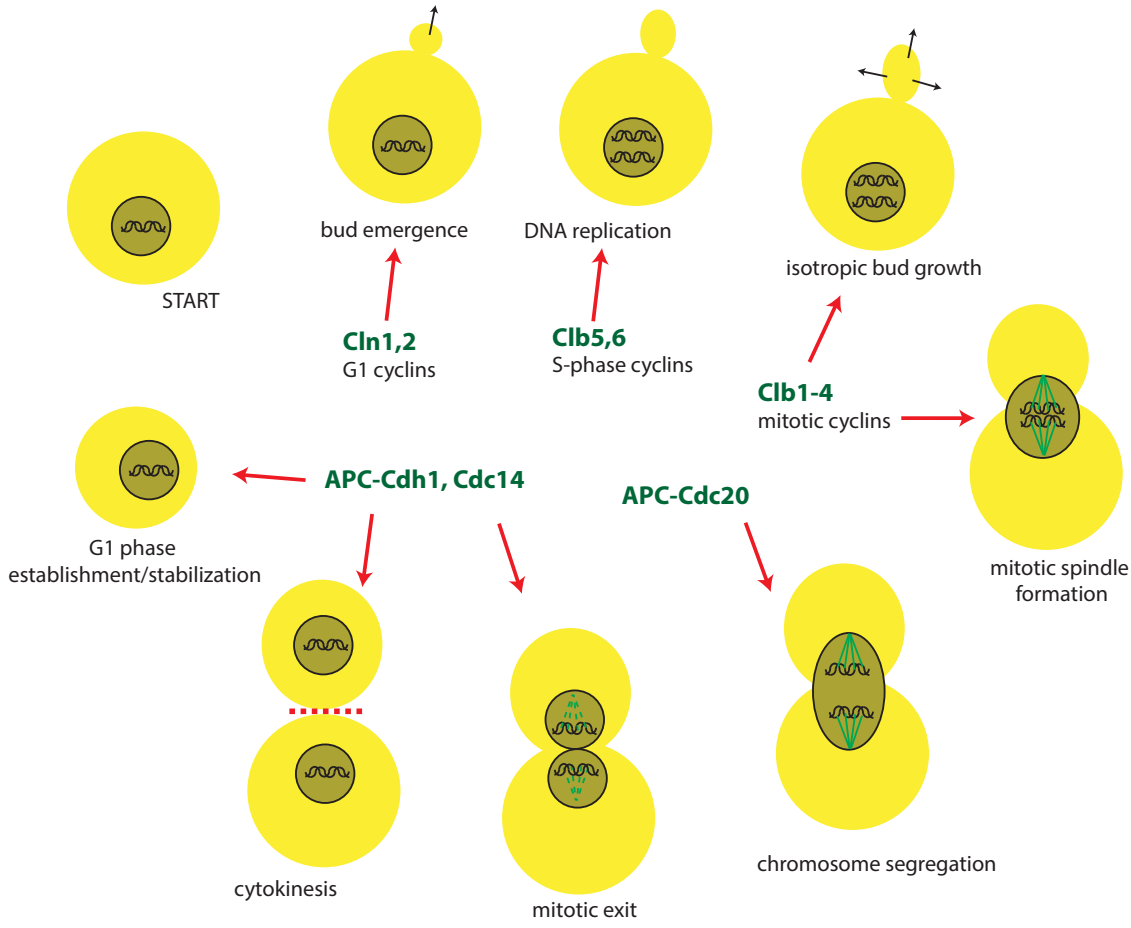

Figure 1.1: Regulation of cell cycle events in budding yeast.

are also responsible for phosphorylation of Sic1, a DNA replication inhibitor (Tyers, 1996). G1 cyclins are highly unstable and Cln-CDK activity drops rapidly upon transcriptional shutoff of the *CLN* genes (Schneider et al, 1998). The second cyclin wave consists of S-phase cyclins, Clb5 and 6, which promote initiation of DNA replication (Epstein and Cross, 1992; Schwob and Nasmyth, 1993). Onset of mitosis is regulated by yet another set of cyclins, Clb1-4, which induce a switch from polarized to isotropic bud growth, duplication of the spindle pole body and formation of mitotic spindle (Amon et al, 1993).

However, in order to complete mitosis, the cyclin-CDK activity must drop, and the drop in CDK activity is mostly ensured by degradation of cyclins. This is achieved by ubiquitylation of cyclins by the anaphase-promoting complex (APC; King et al, 1995; Sudakin et al, 1995). The APC is a multi-subunit protein complex that requires binding of an activator. There are two homologous activators, Cdc20 and Cdh1 (also called Hcm1), which provide timing and specificity (figure 1.2). APC-Cdc20 is active at the metaphase-anaphase transition. Its targets are Clb5, mitotic cyclins, and importantly also securin (Pds1), degradation of which is the first step in the cascade leading to cleavage of cohesin and sister chromatid separation (Cohen-Fix et al, 1996; Shirayama et al, 1999). APC-Cdh1 is activated later, and its main role is stabilizing the G1 phase and ensuring no premature accumulation of mitotic cyclins. Although it is not essential for mitotic exit, its targets also include polo kinase Cdc5, various

components of the mitotic spindle, as well as Cdc20 itself (Hildebrant and Hoyt, 2001; Huang et al, 2001, Schwab et al, 1997).

Another important factor in mitotic exit is phosphatase Cdc14 (Lu and Cross, 2010). Degradation of Clb2 by APC-Cdc20 (Wasch and Cross, 2002) and release of Cdc14 from the nucleolus (Visintin et al, 1999) causes the kinase-phosphatase balance to shift in favor of phosphatase, which drives the mitotic exit (Drapkin et al, 2009).

The difference in timing of these two activators is ensured by cyclin-CDK activity (figure 1.2); Cdc20 preferentially binds to CDK-phosphorylated APC and is therefore active when CDK activity is still high (Rudner and Murray, 2000). In contrast, activity of APC-Cdh1 is activated by the phosphatase Cdc14 (Zachariae et al, 1998) after the balance between phosphatase and kinase activity is shifted in favor of phosphatase.

The regulation of the cell cycle by cyclins, cyclin-dependent kinases, as well as the anaphase-promoting complex and its activators Cdc20 and Cdh1 is conserved among many eukaryotic lineages, including animals and plants. However, a recent study of cell cycle regulation in a highly divergent eukaryote, a human pathogen *Giardia intestinalis*, has revealed that its genome lacks any of the APC components. Furthermore, the only B-type cyclin, while degraded

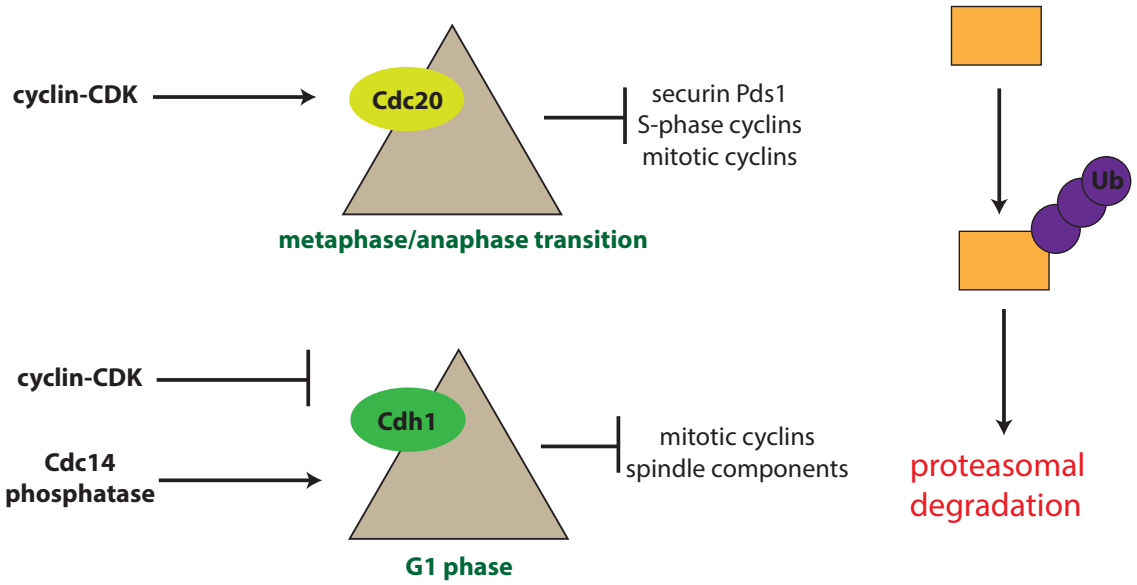

Figure 1.2: Regulation and targets of the anaphase-promoting complex.

during mitosis, is not subjected to ubiquitylation (Gourguechon et al, 2013). Besides this exception, regulation of the cell cycle by cyclin-CDK and the APC is common to eukaryotes.

1.2. Regulation of APC-Cdh1 in budding yeast

In order to allow for accumulation of APC targets that drive the progression through the S-phase and entry into mitosis, it is crucial that the APC activity is restrained after G1-phase. Inactivation of APC-Cdc20 is ensured by its degradation; its degradation is mediated by both APC-Cdh1, as well as other mechanisms (Robbins and Cross, 2010b) to ensure that APC-Cdc20 is not active after the metaphase-anaphase transition. In contrast, activity of APC-Cdh1 is allowed to persist throughout the G1 phase of the next cell cycle and is only inactivated upon cell cycle progression through the G1/S transition (Huang et al, 2001).

The main mechanism of restraining the APC-Cdh1 activity is phosphorylation of Cdh1 at 11 putative CDK consensus sites. Phosphorylation of Cdh1 reduces the ability to bind to the APC, as mutation of phosphorylation sites caused constitutive association of Cdh1 with APC (Zachariae et al, 1998). In addition, it was also suggested that phosphorylation promotes export of Cdh1 out of the

nucleus and sequestration from the APC and its substrates. The export is mediated by a karyopherin Msn5 (Jaquenoud et al, 2002).

It is presently unclear which kinases are responsible for inactivation of APC-Cdh1. An initial study has suggested that G1 cyclins are responsible for inactivation of APC-Cdh1 activity (Amon et al, 1993). Later, it was suggested that Cln-CDKs are not sufficient for APC-Cdh1 inactivation, and Clb3,4,5-CDK are required (Yeong et al, 2001). However, the results of both of these studies were based on stability of ectopically expressed mitotic cyclin Clb2, which is also a negative regulator of APC-Cdh1 in addition to being an APC-Cdh1 substrate. A subsequent study used an inert reporter for APC-Cdh1 activity and found that Clb5 and 6-CDK are responsible for proper timing of APC-Cdh1 inactivation, although APC-Cdh1 inactivation still occurred in absence of Clb5 and 6 (Huang et al, 2001).

Other mechanisms might contribute to APC-Cdh1 inactivation. It was found by mass spectrometry that Cdh1 is phosphorylated at many other residues, which might have regulatory effects (Hall et al, 2004). It was suggested that phosphorylation of Cdh1 by both CDK as well as polo kinase Cdc5 is required for mitotic spindle assembly (Crasta et al, 2008), although mutation of Cdc5 binding sites on Cdh1 was later shown to have no regulatory effects (Robbins and Cross, 2010a). In addition, recognition of substrates by APC-Cdh1 is

blocked by a pseudosubstrate inhibitor Acm1 (Martinez et al, 2006), however, deletion of ACM1 does not have any major effects and inhibition by Acm1 probably plays a relatively minor role. Remarkably, Cdh1 abundance is not significantly regulated by cell cycle-specific expression or degradation and is constant throughout the cell cycle.

Regulation of Cdh1 by multisite phosphorylation is conserved in vertebrates, although the precise localization of phosphorylation sites varies. A stoichiometric inhibitor Emi1 also exists and is regulated in a similar fashion to stabilize mitotic cyclins in interphase and couple DNA replication with mitosis (Di Fiore and Pines, 2007). However, unlike yeast where Cdh1 is stable (Zachariae et al, 1998), Cdh1 is degraded in S-phase by the SCF ubiquitin ligase in mammalian cells (Benmaamar and Pagano, 2005).

A careful study by using exact gene replacements found that unphosphorylatable *CDH1-m11* allele is incompatible with viability (Robbins and Cross, 2010a). Phosphorylation of Cdh1 by CDK is therefore essential for cell cycle progression. Specifically, *CDH1-m11* cells arrest at the G2/M border, with replicated DNA, but before switching to depolarized bud growth and formation of the mitotic spindle. Introducing non-degradable mitotic cyclin Clb2-kd in *CDH1-m11* cells restored the ability to form spindles and depolarize growth, which indicates that in particular restraining the degradation of mitotic cyclins, but not

necessarily other APC-Cdh1 targets, is the main requirement for APC-Cdh1 inactivation (Robbins and Cross, 2010a).

1.3. Multisite phosphorylation in regulation of CDK substrates

Global mapping of CDK substrates in budding yeast has revealed that a large fraction of CDK phosphoproteome consists of substrates that contain multiple CDK phosphorylation sites per protein (Holt et al, 2009). Interestingly, the precise position of these phosphorylation sites is poorly conserved in orthologs in related fungal species. The majority of these sites are found in unstructured regions of proteins and loops. This implies that regulation of these substrates by multisite phosphorylation might often depends on rather non-specific mechanisms that disrupt or enhance protein interactions by adding bulk negative charge on the protein surface (Holt et al, 2009).

Regulation of proteins by multisite phosphorylation has been studied on multiple substrates. An example of regulation by bulk negative charge is Ste5, a scaffold protein involved in MAP kinase signaling in response to mating pheromone. Ste5 is inactivated by Cln-CDK by disrupting its membrane localization (Strickfaden et al, 2007). This is achieved by phosphorylation on a cluster of sites in a basic motif that can bind the plasma membrane. Disruption of

membrane binding requires a large number of negative charges, which is achieved by 8 phosphorylation sites in the plasma membrane binding domain of Ste5 (Strickfaden et al, 2007).

The mechanistically best-understood example of multisite phosphorylation is Sic1, the stoichiometric inhibitor of mitotic cyclin-CDK. Upon phosphorylation, Sic1 is recognized by the SCF ubiquitin ligase and targeted for degradation. An initial study has proposed a “counting mechanism”, in which recognition of the phosphodegron on Sic1 by the SCF ubiquitin ligase is dependent on exactly 6 phosphate groups (Nash et al, 2001). Such mechanism can ensure both a delay as well as a sharp transition, as shown experimentally as well as by a mathematical model (Deshaies and Ferrell, 2001). However, the requirement for six phosphorylation sites was difficult to reconcile with the structure of the human homolog of the SCF bound to cyclin E peptides, where a tight interaction was observed with just a doubly phosphorylated degron (Hao et al, 2007). Subsequently, in sharp contrast to the counting mechanism, a careful biochemical analysis of multisite phosphorylation of Sic1 has revealed an ordered cascade of processive phosphorylation events, initiated by G1 cyclins and then carried out mostly by S-phase cyclin-CDKs (Koivomagi et al, 2011).

Multisite phosphorylation can in principle generate nonlinearity by multiple mechanisms, and such nonlinearity can contribute to generating sharp

transitions between cell cycle stages. Experimentally, nonlinearity was observed and characterized in Xenopus Wee1 (Kim and Ferrell, 2007). Nonlinear response to kinase levels in Wee1 arises through a substrate competition mechanism. Phosphorylation of one critical residue, T150, in Wee1 is highly ultransensitive with response to cyclin B-Cdk1. This nonlinearity arises due to competition with phosphorylation at other inessential kinase sites on Wee1, as well as other high affinity Cdk1 targets (Kim and Ferrell, 2007).

Different phosphorylation sites on the same protein can in principle have different functions. Such a mechanism was described in a budding yeast transcription Pho4, which is phosphorylated by another cyclin-cyclin dependent kinase Pho80/Pho85. Of four phosphorylation sites located on Pho4, phosphorylation at two of the sites promotes nuclear export; phosphorylation at the third site inhibits nuclear import; and phosphorylation at the fourth site prevents association with a binding partner Pho2 (Komeili and O'Shea, 1999). It is an intriguing possibility that such separable roles of different phosphorylation sites might also exist in CDK substrates.

1.4. Cell cycle-regulated gene expression

In parallel to the biochemical oscillator, driven by CDK activity and ubiquitylation, periodic gene transcription also contributes significantly to the cell cycle control. A pioneering study in the late 1990s using the emerging microarray technology has revealed that a significant fraction of yeast genome undergoes cell cycle regulated transcription (Spellman et al, 1998). Overall, about 800-1200 genes (out of ~6400 total) are thought to be statistically significantly upregulated at a certain cell cycle stage (Spellman et al, 1998; Orlando et al, 2008; Pramila et al, 2006; de Lichtenberg et al, 2005). This periodic gene expression is ensured by activity of particular transcriptional factors at different cell cycle stages.

There are three main clusters of gene expression. Transcriptional factors SBF and MBF activate transcription of genes at the G1/S border (Dirick et al, 1992). Among genes in this regulon are G1 cyclins and S-phase cyclins. The second cluster, regulated by transcription factors Mcm1, Fkh1/2 and Ndd1, activates expression of genes at the G2/M border (Koranda et al, 2000). These genes include mitotic cyclins, as well as Cdc20. The third cluster is activated at the mitotic exit, and is regulated by transcription factors Swi5 and Ace2 (Colman-Lerner et al, 2001; Knapp et al, 1996). A few other clusters that contain a smaller number of genes, such as the S-phase cluster regulated by Hcm1

(Pramila et al, 2006), and the histone cluster (Dollard et al, 1994), also contain cell cycle-regulated genes.

It was generally assumed that the activity of these transcription factors is regulated by CDK phosphorylation (or dephosphorylation) and that periodic transcription is therefore downstream of the CDK oscillator. However, a genome-wide study has found that upon depletion of B-type cyclins, cells enter a cell cycle arrest, but the majority of the periodic transcriptome continues to oscillate (Orlando et al, 2008). This hinted that an oscillatory mechanism that is independent of B-type cyclin-CDK activity could sustain periodic transcription. Further study has suggested that even in complete absence of CDK activity, periodic transcription is still present (Simmons-Kovacs et al, 2012). The authors have proposed a model of a transcriptional oscillator, based on sequential activation of transcription factors (Orlando et al, 2008, Simmons-Kovacs et al, 2012). A recent study has proposed that the transcriptional oscillator is stalled when checkpoints are activated (Bristow et al, 2014). It remains unresolved if, and to what extent, periodic gene expression is in fact regulated by periodic cyclin-CDK activity, and to what extent other CDK-independent mechanisms can drive periodic regulation of cell cycle-regulated genes.

1.5. Cell-to-cell variability and effects of molecular noise

Clonal populations of cells can exhibit striking cell-to-cell variability. Expression levels of a gene can vary greatly between genetically identical cells grown in identical environment (Elowitz et al, 2002). Single cell methods to measure protein abundance in single budding yeast cells have showed great variability in abundance of the proteome in budding yeast (Newman et al, 2006). On the level of mRNA, counting single mRNA molecules has revealed substantial variation in number of mRNA molecules per cell (Zenklusen et al, 2008).

This heterogeneity is generally assumed to have no functional significance (reviewed in Altschuler and Wu, 2010). In fact, mechanisms specifically aimed to suppress noise have evolved. For example, in budding yeast cell cycle, an active mechanism of noise suppression was found in the Start transition, where coherence regulatory program was carefully measured in single cells (Bean et al, 2006). Deletion of SWI4, the component of the transcription factor SBF, greatly reduced specifically the cell-to-cell variability in coherence of Start events (time budding and *CLN2* expression peak), but not the mean duration of the interval, consistent with existence of complex mechanisms for noise suppression. The remaining cell-to-cell variability observed in budding yeast Start is perhaps represents a compromise between high coherence of events and high regularity in timing (Bean et al, 2006).

However, in some cases, cells can exploit molecular noise to stochastically generate different transient phenotypic states. So far, these phenomena have mostly been studied in bacteria. For instance, in *Bacillus subtilis*, a fraction of cells can transiently switch to a competent state, during which they can potentially take up foreign DNA from the environment, at the expense of slowing the growth rate. The switching is driven by molecular noise in expression of the regulator (Maamar et al, 2007; Cagatay et al, 2009). A similar phenomenon is seen in *Escherichia coli,* where a small fraction of cells transiently enters a slow growing “persister” state, in which they are less sensitive to lethal doses of antibiotics (Balaban et al, 2004). Such phenomena are seen as bet hedging; the population sacrifices its fitness to gain phenotypic diversity, which increases the chance of survival in unpredictable environments. Bet hedging can provide an advantageous strategy for survival to simple sensing and responding to changes in environment (Kussell and Leibler, 2007).

A possibly related phenomenon was recently also observed in budding yeast. High throughput imaging has revealed that clonal populations of yeast cells exhibit a range of growth rates (Levy et al, 2012) in a heritable manner. It was found that slower growth correlates with resistance to heat killing and correlates with age. While the significance of this phenomenon is not yet fully understood, it might be another example of a similar bet-hedging strategy that could ensure population survival in unpredictable environments (Levy et al, 2012).

In the budding yeast cell cycle, duration of various events of cell cycle differs substantially between cells. Much of this variability is accounted for by the duration of G1 phase (Lord and Wheals, 1981). The variability of G1 phase can be partially attributed to molecular noise; coefficient of variation of the duration of the unbudded period of the cell cycle (cytokinesis to bud emergence) scales with the square root of ploidy, suggesting that molecular noise in gene expression is an important source of variability in G1 phase (Di Talia et al, 2007). However, additional element controlling the variability of the duration of G1 is cell size at birth in daughter cells. Due to asymmetric cell division, daughter cells are born smaller and more variable in size. Since cell size control is executed in G1, the duration of the G1 phase in daughters is also highly dependent on cell size at birth (Di Talia et al, 2007). In contrast, little is understood about variability of the duration of the budded period of the cell cycle, which is also significantly variable.

1.6. Rationale for the present study and organization of the thesis

The aim of the present study was to gain understanding into the variability of the budding yeast cell cycle and regulation of Cdh1 inhibition by multisite phosphorylation. As outlined above, many questions about regulation of APC-

Cdh1 remain unresolved, and understanding the regulation of proteins by multisite phosphorylation is of significant general interest.

All the work was done in the budding yeast Saccharomyces cerevisiae. In chapter 2, I focus on development of a quantitative assay to measure the dynamics of APC-Cdh1 activity in single cells, and address the cell-to-cell variability of timing of cell cycle events leading to entry into mitosis. In subsequent chapters 3 and 4, I then focus on regulation of Cdh1. In chapter 3, I address the regulation of APC-Cdh1 by multisite phosphorylation by generating partially phosphorylatable *CDH1* mutants and analyzing their phenotype. In chapter 4, I focus on the relationship and hierarchy between regulators of Cdh1. Chapter 5, experimental part of which was done in collaboration with S. Jamal Rahi and Kresti Pecani, is a departure from the topic of the rest of this thesis, and is an analysis of the genome-wide pattern of cell cycle-regulated gene expression, also in Saccharomyces cerevisiae. Chapter 6 is a discussion of the main findings of the work presented in the thesis.

Chapter 2: Timing of mitotic entry events

2.1. Variability of duration of the budded period of the budding yeast cell cycle

The budded period of the cell cycle (time from bud emergence to cytokinesis) is variable (Di Talia et al, 2007; figure 2.1). In contrast to the G1 period, the variability does not scale with ploidy, ruling out the molecular noise in gene expression as a simple explanation (Di Talia et al, 2007). The variability is also not accounted for by sporadic activation of checkpoints, since deleting both the components of the spindle assembly checkpoint and DNA damage checkpoint at once does not reduce the variability (F. Cross, unpublished data).

The budded period of the cell cycle involves multiple crucial cell cycle events and independent regulatory steps, and it remains unexplored how variable each of these steps are. In this chapter, I focused on developing tools to assess the timing and variability of regulatory events leading to entry into mitosis, inactivation of APC-Cdh1 and activation of expression of the mitotic cyclin *CLB2*.

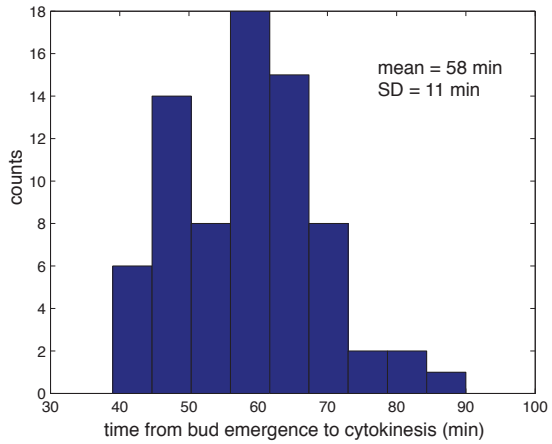

Figure 2.1: Variability of the budded period in the budding yeast cell cycle. A histogram of durations of the cell cycle period from budding to cytokinesis, as measured by presence of the bud neck marker Myo1-mCherry signal at the bud neck.

2.2. Development of a biosensor for APC-Cdh1 activity

In order to precisely measure the variability in inactivation of APC-Cdh1, I sought to develop a fluorescent biosensor that would be sensitive to degradation regulated by ubiquitylation by APC-Cdh1. An ideal biosensor would be inert and degraded exclusively by APC-Cdh1.

Based on these considerations, I constructed the biosensor using a C-terminal fragment of Ase1, a spindle protein (Juang et al, 1997). Unlike many other APC targets that are ubiquitylated by both APC-Cdc20 and APC-Cdh1, Ase1 is strongly destabilized by APC-Cdh1, but is not significantly destabilized by APC-Cdc20 (Visintin et al, 1997). Previous studies have also determined the minimal Ase1 fragment necessary and sufficient for degradation and established that this fragment does not interfere with any cellular processes (Huang et al, 2001).

The construct encoded the C-terminal fragment of Ase1 sufficient for APC-Cdh1 degradation (amino acid residues 632-885) fused to a yellow fluorescent protein yVenus and placed the construct under control of the *MET3* promoter (figure 2.2 A). *MET3* promoter is repressed by methionine in the media and expressed in absence of methionine. Expression from the *MET3* promoter has been shown to be stable throughout the cell cycle (Charvin et al, 2008).

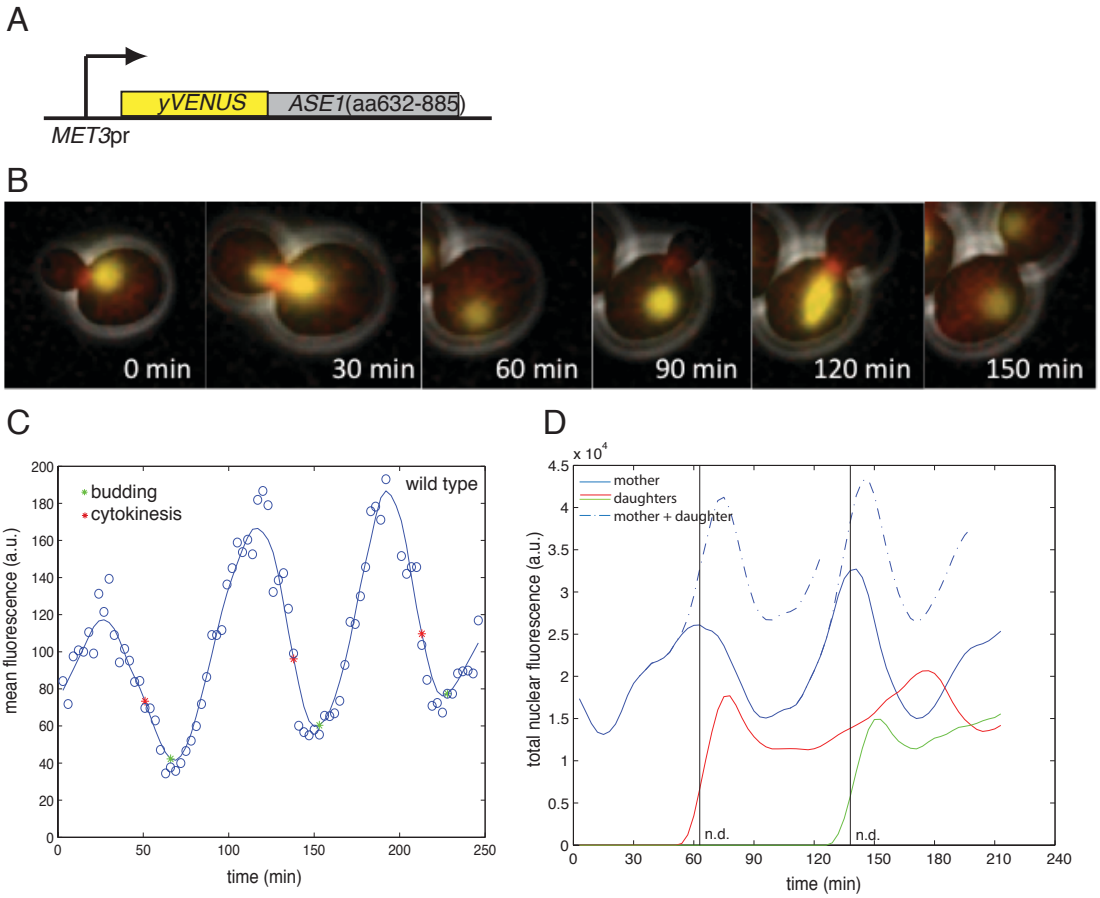

Figure 2.2: A biosensor for APC-Cdh1 activity. A) A scheme of the biosensor construct. The construct is composed of a fusion of a yellow fluorescent protein (yVenus) and the C-terminal sequence of Ase1. Expression of the construct is driven by the methionine-repressible promoter *MET3*pr. B) Combined phase-contrast and fluorescence images from the time-lapse video of a representative wild-type cell expressing the biosensor (yellow) and a bud-neck marker Myo1-mCherry in red. C) Quantification of mean cellular fluorescence in a representative cell expressing the biosensor. Open circles: raw data, solid line: smoothing spline fit. D) Quantification of total nuclear fluorescence in a representative cell. Black lines represent nuclear division, and dashed line is the sum of the fluorescence in the mother and daughter nucleus.

The cells carrying the biosensor exhibited once per cell cycle oscillations in yVenus fluorescence (figure 2.2 B). To quantitatively assess these oscillations, I quantified mean cell fluorescence by using the semi-automated image segmentation software (Charvin et al, 2008). The fluorescence begins to rise around the time of bud emergence, and conversely, fluorescence begins to drop before cytokinesis (figure 2.2 C). These oscillations of fluorescence are due cell cycle-regulated stability of the biosensor by APC-Cdh1. However, an effect, owing to the fact that the biosensor is localized in the nucleus, contributes to the mean fluorescence of the cell. At the time of the nuclear division, half of the amount of the biosensor was lost to the nascent daughter cell during the nuclear migration and division (and was excluded in quantification of the mother cell), resulting in a drop of fluorescence in the mother cell. Since APC-Cdh1 activity is present at mitotic exit, the timing of these two effects is somewhat overlapping.

To account for that effect due to nuclear division and demonstrate that degradation of the biosensor indeed takes place, I quantified the total fluorescence of the nucleus, corresponding to the total amount of the biosensor (figure 2.2 D). To account for fluorescence loss at nuclear division, I then summed up the fluorescence of the mother and daughter cells after nuclear division (dashed lines). The total fluorescence still dropped after the nuclear division, indicating that biosensor was degraded after nuclear division. However,

the dynamic range of oscillations was reduced if the dilution of fluorescence due to nuclear division was taken into account.

It needs to be noted that the gradual rise and fall, rather than sharp transitions in fluorescence levels, are due to slow maturation time of fluorescent proteins; first order constant for maturation of yVenus in budding yeast was measured to be around 20 minutes (Charvin et al, 2008). Assigning precise transition times from such gradual changes poses a problem. I tackle this issue later in this chapter; I note that the problem is analogous to determining turn-on times of promoters, which are likewise masked by identical dynamics of slow fluorescent protein maturations (Skotheim et al, 2008).

2.3. Oscillations in biosensor stability are due to APC-Cdh1 activity

First, I sought to establish whether constant activity of APC-Cdh1 is sufficient for complete biosensor degradation. To do so, I measured the biosensor dynamics in cells lacking the ability to inhibit APC-Cdh1 activity. I used an unphosphorylatable and therefore constitutively active allele of *CDH1*, *CDH1-m11*, that lacks all 11 CDK phosphorylation sites (Robbins and Cross, 2010a; Zachariae et al, 1998). *CDH1-m11* is lethal, but cells can be conditionally kept alive by overexpressing *ACM1*, the stoichiometric inhibitor of APC-Cdh1, from a galactose-inducible promoter. Upon switch to glucose to turn off *GAL-ACM1*,

CDH1-m11 cells arrested at mitotic entry. In these arrested cells, the biosensor fluorescence was very low and constant (figure 2.3 B,C). The constant fluorescence indicates a steady state with balanced synthesis and high degradation rate, as the expression from *MET3* promoter persists during the arrest. This result indicates that constitutive activity of APC-Cdh1 is sufficient for constant high degradation rate of the biosensor.

I then sought to establish whether Cdh1 is solely responsible for cell cycle-regulated degradation of the biosensor. To do that, I examined the dynamics of the biosensor in cells lacking APC-Cdh1 activity. *cdh1* cells are viable and do not exhibit any major cell cycle defects. Quantified as mean fluorescence within the entire cell boundary (excluding the bud), the biosensor fluorescence was substantially (three-fold) elevated throughout the cell cycle compared to wild type, indicating an overall lower degradation rate in these cells (figure 2.3 C). Therefore, APC-Cdh1 contributes to degradation of the biosensor.

However, quantifying the fluorescence as mean fluorescence within the entire cell still results in oscillations during the cell cycle, with fluorescence dropping precipitously at the time just before cytokinesis (figure 2.3 A). This is due to the nuclear localization effect, described above. To account for that, I instead quantified the total fluorescence of the nucleus in *cdh1* cells (figure 2.3 D), similarly as done above for wild type cells (figure 2.2 D). The sum of

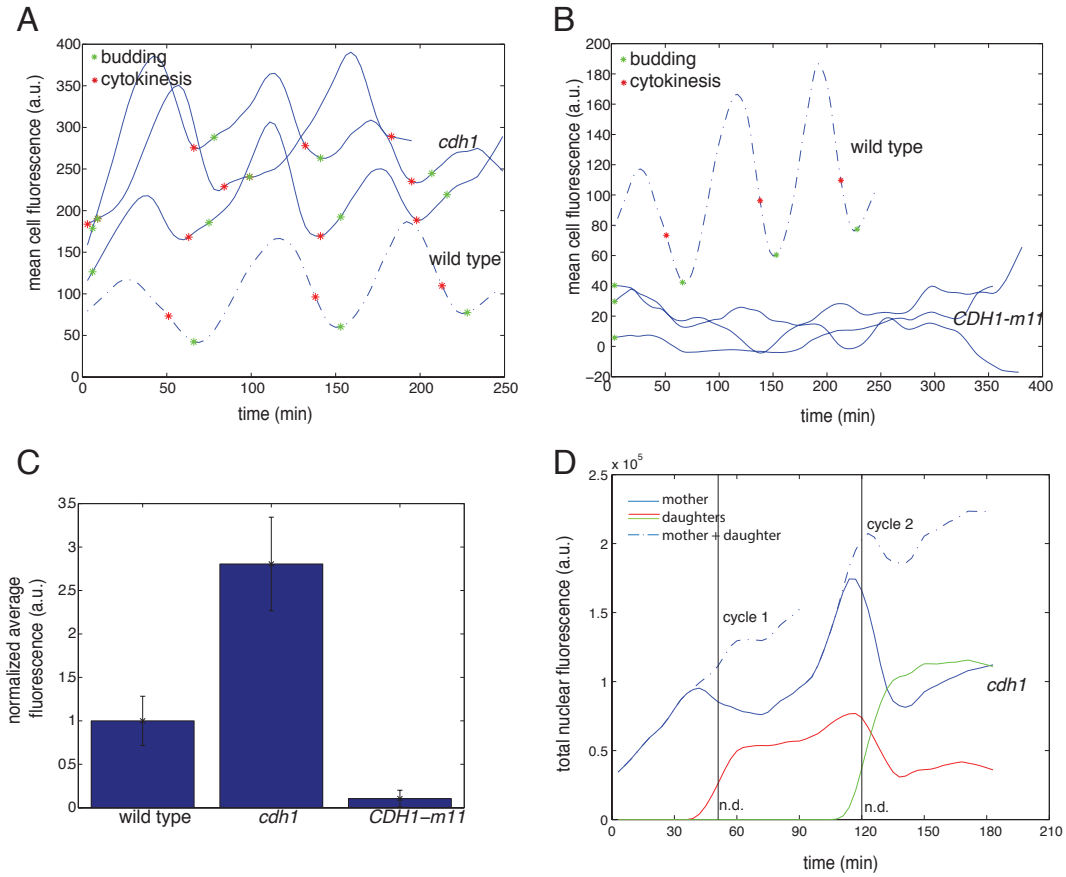

Figure 2.3: APC-Cdh1 is responsible for oscillations in biosensor fluorescence. A) Representative traces of biosensor fluorescence in *cdh1* cells, along with a wild type cells (dashed line). B) Representative traces of biosensor fluorescence in *CDH1-m11* cells. C) Quantification of normalized average fluorescence levels. D) Representative traces of biosensor fluorescence in *cdc20* cells. Fluorescence values shown in these plots were corrected for autofluorescence by subtracting fluorescence values of unlabeled cells.

fluorescence of the mother and daughter nuclei after nuclear division resulted in a linear rising trend, consistent with constant synthesis of the biosensor, in most cell cycles (71% of cell cycles; example cycle 1 in figure 3.3 D). Only in a minority of cell cycles (29%) the summed fluorescence of the mother and daughter nuclei exhibited a slight drop. This effect could be attributed to image analysis, since the total fluorescence intensity of the nucleus is difficult to quantify due to changing shape of the nucleus during the division.

2.4. Determining the timing of APC-Cdh1 inactivation in single cells

In this work, I wanted to develop a method to determine the time of inactivation of APC-Cdh1. However, this problem is challenging because slow maturation time of fluorescent proteins masks the sharpness of transitions. The problem is analogous to examining promoter turn-on times, for which tools already exist (Skotheim et al, 2008; Eser et al, 2011).

Previously, the maximum of the second derivative of the smoothing spline fit was used for determining the turn-on time for a promoter (Skotheim et al, 2008). However, for the biosensor data, it turned out that the second derivative method is particularly sensitive to noise in fluorescence measurements (see chapter 2.6). Subsequently, a method for determining the turn-on times from where the

first derivative reaches 10% of the maximum value has been used (Eser et al, 2011), as it was shown that this method provides higher reproducibility between datasets (Jan Skotheim, personal communication).

I measured the APC-Cdh1 turn-off times from the fluorescence time series quantified as mean cell fluorescence. Since the nucleus is divided earlier in the cell cycle, the effect of the nuclear division does not interfere with the determination of APC-Cdh1 inactivation time. In order to assign a sharp timing of the APC-Cdh1 inactivation from the data with gradual rise of fluorescence, the time point at which the first derivative of the smoothing spline fit changed from negative to positive (i.e. where the slope turns upwards) was chosen to be assigned as the APC-Cdh1 turnoff time. I note that the method used here is essentially equivalent to the 10% of the maximum of the first derivative method, since the first derivative of APC-Cdh1 biosensor traces typically reaches about 10% around the first frame after the fluorescence minimum (figure 2.5); therefore the difference between the results of these two methods would be smaller than the sampling interval.

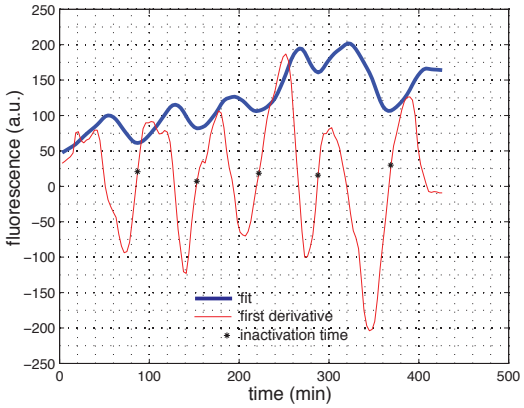

Figure 2.4: A first derivative-based method for detection of APC-Cdh1 inactivation time. Bold blue line: a smoothing spline fit of a fluorescence trace as shown in 2.2. Red line: first derivative of the fluorescence trace, computed as difference between fluorescence values at two adjacent time points. Black stars: points of the transition as determined by the algorithm. The points where the first derivative transitioned to positive represent APC-Cdh1 inactivation times.

2.5. Measuring the contribution of measurement error to the timing of APC-Cdh1 inactivation

It is unclear to what extent the determination of the measured inactivation time is governed by the noise. The fluorescence intensities measured from images vary considerably between frames, and the noise at particular time points could strongly affect the exact shape of the smoothing spline fit, the first derivative function, and the measurement of the APC-Cdh1 inactivation time.

To estimate the noise, I calculated the difference between the raw data value and the value of the corresponding fit at each data point of the curve. The distribution of the difference is uniform throughout the time course and follows a roughly normal distribution (figure 2.5, panels A,B).

I then added normally distributed noise (with the same standard deviation as the SD for the difference between the raw data and smoothing spline fit) to the smoothing spline fit (figure 2.5 C). This generated simulated data with equal degree of noisiness as the raw data. Then, I fitted the simulated data with a smoothing spline, and determined the apparent APC-Cdh1 inactivation time from the fitted simulated data using the first derivative method.

Figure 2.5: Estimation of measurement noise in inactivation time. A,B) The distribution of the difference between the raw data and the smoothing spline fit. C) The procedure for generating simulated data. Raw data (thin blue line) was fitted with the smoothing spline (bold blue line). Subsequently, random noise with the standard deviation of the distribution in B was added (thin red line). Simulated data was then fitted again with the smoothing spline (bold red line) and inactivation times were determined as in 2.4. D,E) Examples of fluorescence traces for two cell cycles. Blue line, smoothing spline fit; blue dots, raw data. Inset, the distributions of measurement error in APC-Cdh1 inactivation, defined as the difference in time measured from the simulated data and the time measured from the experimental data, by generating the simulated data 50 times. The data for the cell in D) represent a noise-resistant measurement. The measurement for the cell in E) is sensitive to noise, and was discarded.

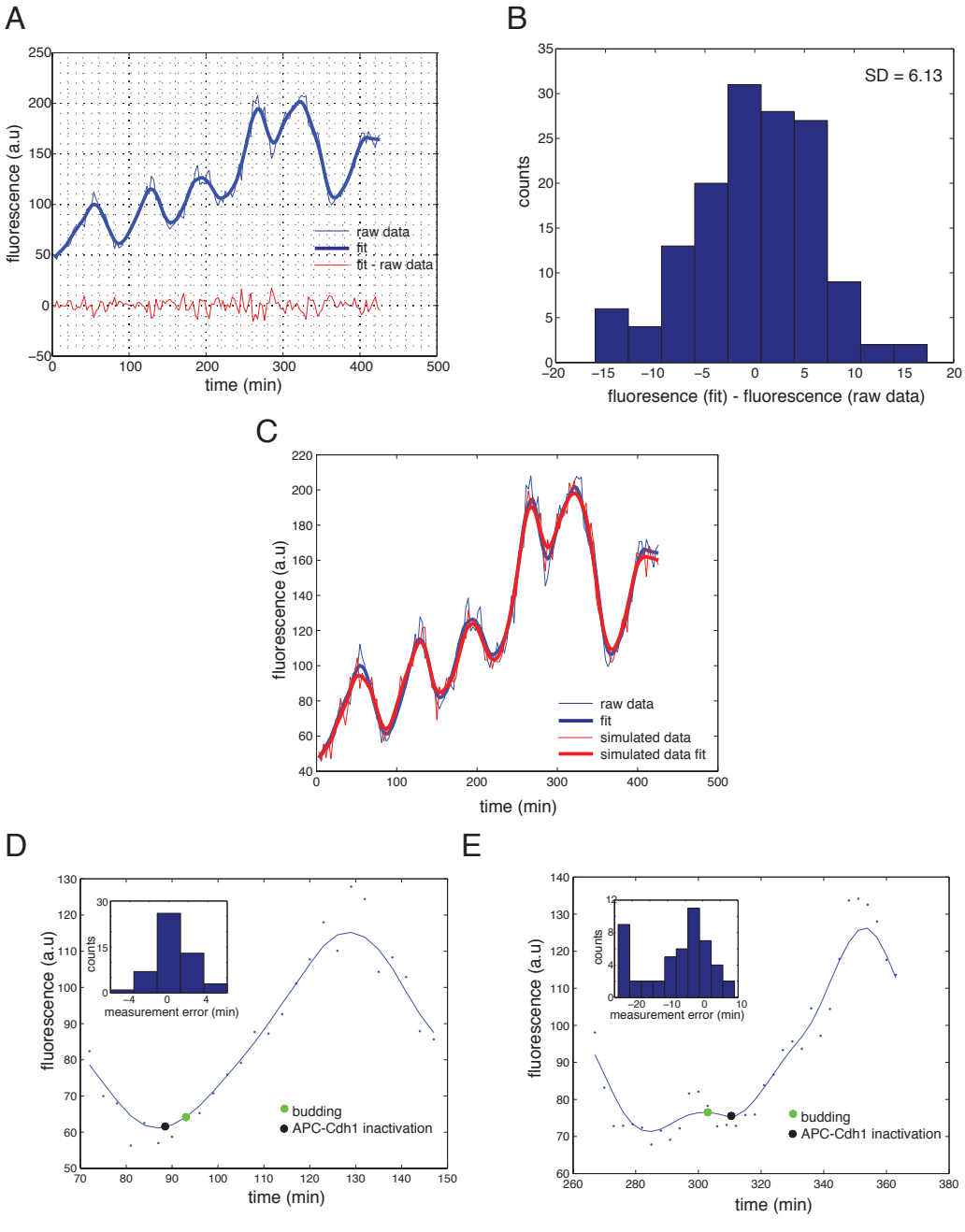
A
fluorescence (a.u)
time (min)
raw data
fit
fit - raw data
B
SD = 6.13
counts
fluoresence (fit) - fluorescence (raw data)
C
fluorescence (a.u)
time (min)
raw data
fit
simulated data
simulated data fit
D
fluorescence (a.u)
time (min)
counts
measurement error (min)
budding
APC-Cdh1 inactivation
E
fluorescence (a.u)
time (min)
counts
measurement error (min)
budding
APC-Cdh1 inactivation

The difference between the time of inactivation measured from the fit of the simulated data and the time of inactivation measured from the original fit represents the measurement error. For each cell, I performed the procedure multiple times to obtain a distribution of the apparent APC-Cdh1 inactivation measurement error (figure 2.5 D,E). I define the mean of the measurement error (MME) to be the mean of this distribution, and the standard deviation of the measurement error (SDME) to be the standard deviation of this distribution.

For most cells, the distribution of measurement error was tight and centered around 0 (figure 2.5 D). However, a fraction of measured cells was found to be sensitive to noise, as the SDME was significantly bigger than zero (indicating a great dependence of the measurement to noisy time points), and/or the MME differed greatly from zero (indicating a systematic shift in the measurement of APC-Cdh1 inactivation; figure 2.5 E). The fluorescence traces of these cells typically had a less sharp transition, which could be due to some noisy time points around the time of transition (figure 2.5 E). The apparent APC-Cdh1 inactivation time from these cell cycles therefore does not represent an accurate measurement of the biological event. To avoid contaminating the measurement of cell-to-cell variability with potentially noisy data points, I excluded cell cycles in which the MME was greater than 3 minutes, or in which the SDME was greater than 3 minutes. By using this procedure, I therefore limited the contribution of the measurement error to the standard deviation to maximum 3

minutes, and the rest of the measured standard deviation therefore likely reflects biological variability. The 3 minutes cutoff is equal to the imaging frequency in the experiment; therefore detection of events on a shorter time scale in this experiment is impossible.

I note that exclusion of a fraction of cells might potentially introduce a bias, because it is possible that these excluded cells might include a population of biologically different cells, for instance cells in which APC-Cdh1 inactivation was less sharp. However, the number of excluded cells in the experiments was only 10-20% (table 2.1), and the excluded cells looked morphologically normal and had overall similar cell cycle times.

2.6. Variability in timing of APC-Cdh1 inactivation

Using a strain that harbored a fluorescently labeled Myo1-mCherry as a bud neck marker in addition to the APC-Cdh1 biosensor, I measured the time of APC-Cdh1 inactivation with respect to budding. On average, Cdh1 was inactivated 4 minutes before budding (figure 2.6 A). However, even after removing the noisy data points using the procedure described above, there was a considerable variability between cells, likely representing biological cell-to-cell variability in coherence between these two events. This poor coherence

between budding and APC-Cdh1 inactivation could be due to variability in APC-Cdh1 inactivation times, variability in timing of bud emergence (already known to be variable (Di Talia et al, 2007)), or both.

To measure the timing of APC-Cdh1 inactivation with respect to relevant regulatory steps, I constructed a strain carrying both the APC-Cdh1 biosensor, as well as a GFP-tagged Whi5 protein. Whi5 is a transcriptional repressor that controls the passage through Start, the commitment point in the budding yeast cell cycle. Whi5 directly represses the G1/S transcriptional regulon, which includes all of the regulators of Cdh1 – *CLN1,2, CLB5,6* and *ACM1*. Upon phosphorylation of Whi5, the repression is lifted and the G1/S regulon transcription can occur. At the same time, Whi5 localization sharply changes from nuclear to cytoplasmic, which can be followed by time-lapse microscopy.

APC-Cdh1 inactivation occurred 12 minutes after Whi5 nuclear exit (figure 2.6 B), and variability between cells is considerably smaller than when measured with respect to Whi5 exit than to budding. The standard deviation is only 3 minutes, which is equal to the upper estimate of the fitting error. Since the frame rate in the experiment was also 3 minutes, and that measurement of Whi5 exit is limited by this estimate, the measurement effectively limits the variability to one frame. Therefore, I cannot exclude that there might not be any biological variability between cells at all.

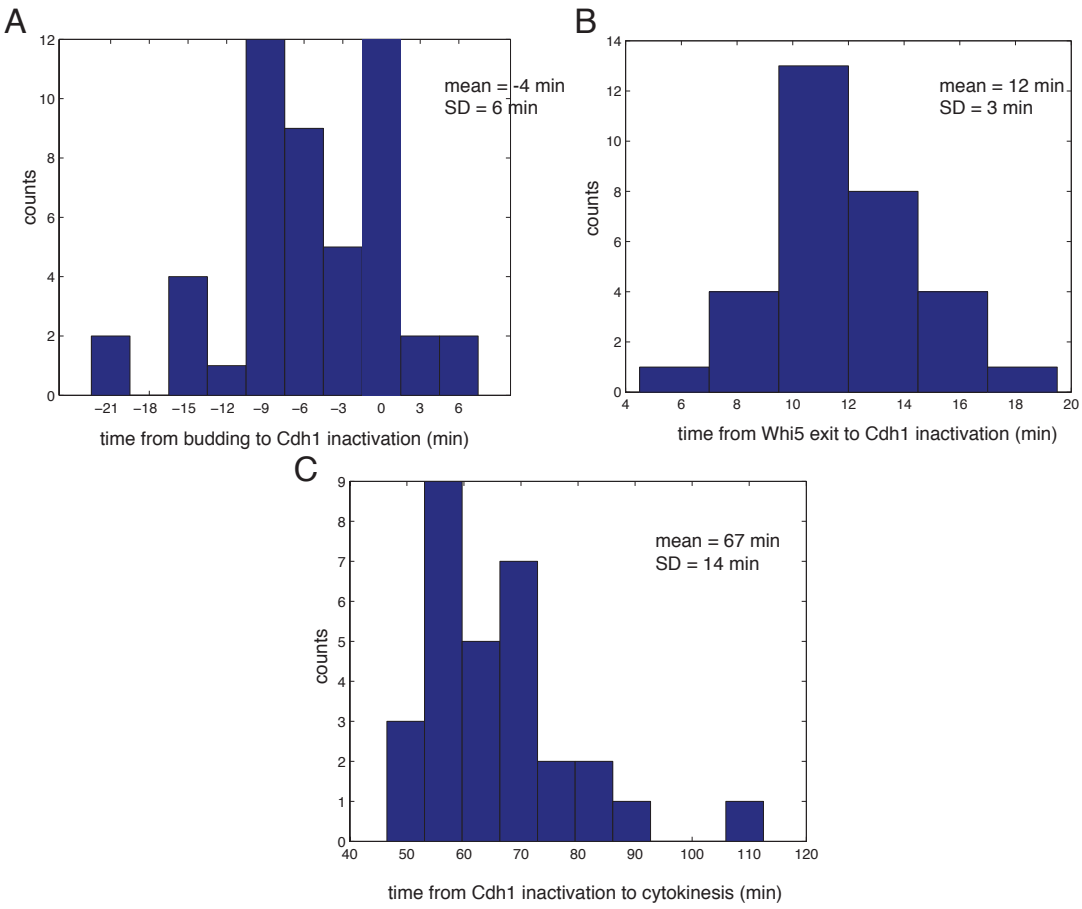

Figure 2.6: Timing of APC-Cdh1 inactivation with respect to cell cycle events. A) A histogram of times from budding to APC-Cdh1 inactivation. B) A histogram of times from Whi5 nuclear exit to APC-Cdh1 inactivation. C) A histogram of times from APC-Cdh1 inactivation to cytokinesis. Each data point represents a measurement from one single cell. The data points that were sensitive to noise are excluded.

I also measured the time of APC-Cdh1 inactivation with respect to subsequent cytokinesis (detected by disappearance of the Myo1-mCherry signal at the bud neck; figure 2.6 C). Compared to the variability of the time from budding to cytokinesis, APC-Cdh1 inactivation occurred with similar variability (table 2.1). It is therefore likely that the timing of APC-Cdh1 inactivation is not the crucial factor in the post-budding variability in the cell cycle timing.

2.7. Variability in timing of *CLB2* promoter activation

I measured the timing of another event leading to entry into mitosis, activation of *CLB2* promoter. Accumulation of the mitotic cyclin Clb2 requires APC-Cdh1 inactivation (Robbins and Cross, 2010a). The expression of mitotic cyclin genes is cell cycle-regulated; the *CLB2* gene belongs to the *CLB2* cluster (Spellman et al, 1998). It is believed that mitotic cyclin-CDK activity is required for full activation of *CLB2* (Amon et al, 1993). Consistent with the existence of such positive feedback loop, I show later in this work that inactivation of APC-Cdh1 is required for *CLB2* promoter expression, as cells bearing constitutively active *CDH1-m11* do not activate the *CLB2*pr (chapter 3.8). It is therefore expected that induction of *CLB2* expression occurs after APC-Cdh1 inactivation.

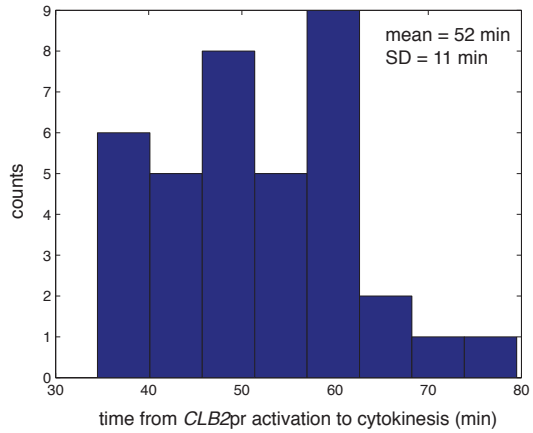

Figure 2.7: Timing of *CLB2*pr induction. A histogram of times from *CLB2*pr induction to cytokinesis.

To measure the time of induction of *CLB2* promoter, I used a construct of *CLB2* promoter driving the expression of unstable GFP (Skotheim et al, 2008). The strain also harbored the *MYO1*-mCherry bud neck marker for detection of cytokinesis.

Using these two markers, I measured the time from *CLB2*pr activation to subsequent cytokinesis. I determined the *CLB2*pr activation time using the same first derivative-based detection method, and applied the same procedure as used for the APC-Cdh1 biosensor to address the dependence of each data point to noise (see chapter 2.5). The *CLB2*pr-GFP signal exhibits a lower dynamic range; as a result, the measurements of induction times from the first derivative sign switch in this experiment were more dependent on noise. I included data points from cell cycles for which both the MME and SDME were less than 4.5 minutes (as opposed to 3 min for the APC-Cdh1 biosensor experiments). This causes a bigger residual error in these measurements.

On average, *CLB2*pr activation occurred later than APC-Cdh1 inactivation (comparing both events with respect to cytokinesis; figure 2.7, table 2.1). In addition, the timing of the interval from *CLB2*pr inactivation to cytokinesis is variable. This raises the possibility that the entire variability of the post-Start

period of the cell cycle could be accounted for by variability of events after *CLB2*pr induction.

2.8. Conclusions and future directions

In this chapter, I focused on developing experimental tools and data analysis procedures to measure the timing of cell cycle events that lead to entry into mitosis. These tools enabled quantitative measurement of cell-to-cell variability of these events. This work was motivated by the fact that variability of the duration of the cell cycle period after budding is not understood. I therefore sought to measure the durations of various sub-periods, with the idea that finding sub-periods of the cell cycle that are not variable in timing would allow me to narrow down the cell cycle events that are responsible for generating variability.

In general, variability of timing of different events is different to compare because of technical error; biological variability is masked by measurement variability. The detection of events is limited by sampling resolution (3 minutes in all experiments presented here) and is additionally increased for events of which timing was extrapolated by the first derivative method. This causes a technical error in the measurements. In general, a useful parameter for comparison of

variability for events with different average durations is coefficient of variation (CV; ratio of standard deviation (SD) over mean), because it takes into account the average duration of events. However, technical variability due to sampling resolution is independent of the mean, and therefore affects longer events less than shorter events (assuming equal CV). CV is therefore only useful for comparing longer events. In contrast, for shorter events, comparing SD (assuming the technical error is the same for both events) might be more useful. However, this comparison is only valid for events of equal mean duration.

The findings are schematically summarized in figure 2.8. Timing of bud emergence is independent of all other events, since budding is regulatorily decoupled from other events assessed here. Therefore, the relevant reference point for measurements is Whi5 exit, which marks the Start transition. Start is the major regulatory step that controls both bud emergence and APC-Cdh1 inactivation. The timing of bud emergence with respect to Start is variable (Di Talia et al, 2007; table 2.1) and ploidy dependent, suggesting that it is affected by molecular noise in gene expression (Di Talia et al, 2007). In contrast to budding, the timing of APC-Cdh1 inactivation was found to be invariable with respect to Start (table 2.1). I did not test whether the variability in timing of APC-Cdh1 inactivation is ploidy-dependent. The standard deviation reported for the interval from Whi5 exit to APC-Cdh1 inactivation is an overestimation of the actual biological variability, because it still includes the remaining measurement

error in APC-Cdh1 inactivation (the upper limit is 3 minutes) as well as error in detection of Whi5 exit, which is limited by the imaging interval (also 3 minutes). Given these technical constraints, the contribution of (biological) cell-to-cell variability might be as low as zero. This is in contrast to the variability of APC-Cdh1 inactivation with respect to budding, which on average occurs at almost the same time, but has considerable cell-to-cell variability.

Inactivation of APC-Cdh1 depends on multiple genes expressed from the G1/S regulon: *CLN1,2, CLB5,6* and *ACM1* are all SBF and MBF targets. *CLN2* promoter expression is almost concurrent with Whi5 exit, measured in single cells (Skotheim et al, 2008). Expression of most other members of the regulon occurs later than *CLN2* (Eser et al, 2011), but can be expected to be expressed with little cell-to-cell variability in timing (like *CLN2*), although no single cell data exists for the particular APC-Cdh1 regulator genes. Deletion of *WHI5* advances expression of the regulon (Skotheim et al, 2008); it would be interesting to assess whether it also advances APC-Cdh1 inactivation. Furthermore, to test whether the timing of APC-Cdh1 inactivation is dependent specifically on SBF or MBF-regulated transcripts, it would be interested to measure the time of APC-Cdh1 inactivation in cells where either MBF or SBF are removed by deleting the DNA-binding domains of those transcription factors, *MBP1* and *SWI4*, respectively.

Event	Mean (min)	SD (min)	CV	Number of cells measured	Number of cells excluded
Bud emergence to cytokinesis	58	11	0.19	74	0
Bud emergence to APC-Cdh1 inactivation	-4	6	1.5	49	6
Whi5 exit to APC-Cdh1 inactivation	12	3	0.25	31	10
APC-Cdh1 inactivation to cytokinesis	67	14	0.21	30	5
*CLB2*pr activation to cytokinesis	52	11	0.21	37	15
Whi5 exit to bud emergence	23	10	0.43	66	0

Table 2.1: Summary of the data from chapter 2. The last column is the number of cells that were excluded from the measurement due to sensitivity to experimental noise.

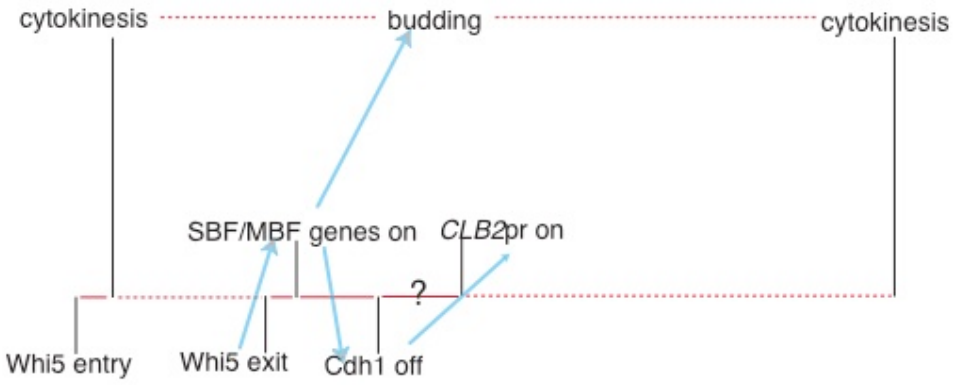

Figure 2.8: Variability in cell cycle events. A schematic representation of the findings in this chapter, in combination with results from Di Talia et al, 2007 and Skotheim et al, 2008. The dotted lines represent intervals that show considerable cell-to-cell variability in duration; solid lines represent cell-to-cell invariable intervals. The question mark represents a hypothesized invariable interval (see text). Blue arrows are known regulatory nodes.

Another event of interest is activation of APC-Cdh1 at mitotic exit. APC-Cdh1 is activated by dephosphorylation by phosphatase Cdc14 (Visintin et al, 1997; Lu and Cross, 2010). The timing of Whi5 nuclear entry, which is also regulated by Cdc14 dephosphorylation of Whi5, was measured to occur 6 minutes before cytokinesis with little or no cell-to-cell variability (Di Talia et al, 2007; K. Pecani, unpublished data), and it is likely that APC-Cdh1 is activated with similar dynamics. Measuring the timing of APC-Cdh1 activation would have to take into account the drop in fluorescence due to nuclear division (which occurs at around the same time).

I also examined the timing of activation of *CLB2* promoter. The cell-to-cell variability in time from *CLB2*pr induction to cytokinesis is equal to the variability of time from budding to cytokinesis. Therefore, the entire variability of the budded period of the cell cycle can be explained by the variability from *CLB2*pr activation to cytokinesis. Since I show that inactivation of APC-Cdh1 is required for *CLB2*pr activation (see chapter 3.8), I speculate that the entire regulatory set of events leading from Start to APC-Cdh1 inactivation to induction of *CLB2* expression might be invariable in timing. Directly measuring the time between APC-Cdh1 inactivation and *CLB2*pr activation in the same cell would reveal if this timing interval is invariable. If this interval is indeed found to be constant, this would suggest a deterministic chain of events leading from Start to APC-

Cdh1 inactivation to *CLB2* expression, which leaves entire post-Start variability to be generated by events after *CLB2*pr induction.

A general future direction is further dissection of the variability of cell cycle events after *CLB2*pr activation. I propose measurement of timing of a further set of cell cycle events, such as markers for transcriptional activity of genes that regulate the S-phase, chromosome segregation, and mitotic exit, both with respect to budding and cytokinesis, as well as with respect to each other. Using multiple transcriptional markers in the same cell should be possible by combining spectrally non-overlapping fluorescent proteins. Taken together, these measurements should be able to narrow down and define intervals that generate the observed variability, as well as provide a basis for further studies into mechanisms that generate and/or suppress variability in the budding yeast cell cycle.

Chapter 3: Analysis of multisite phosphorylation of Cdh1

In this chapter, I investigate the mechanism of APC-Cdh1 inactivation by multisite phosphorylation. There are 11 putative CDK phosphorylation sites on the Cdh1 protein (figure 3.1; Zachariae et al 1998, Robbins & Cross 2010a). In complete absence of CDK phosphorylation, Cdh1 remains associated with the APC and active (Zachariae et al, 1998). Exact gene replacement of the *CDH1* gene with an allele lacking all 11 phosphorylation sites, *CDH1-m11*, at the endogenous locus, confirmed that unregulated *CDH1-m11* is incompatible with viability due to the inability to restrain the APC-Cdh1 activity at the entry into mitosis (Robbins and Cross, 2010a). Cells bearing the unphosphorylatable *CDH1-m11* allele entered the S-phase and underwent one round of DNA replication normally, but failed to depolarize bud growth and form mitotic spindles. These defects were found to be due to unrestrained Clb2 proteolysis (Robbins and Cross, 2010a).

A correlation between the number of CDK phosphorylation sites on Cdh1 and the ability to suppress degradation of mitotic cyclins has previously been reported (Zachariae et al, 1998). However, the study relied on overexpression of Cdh1, which is problematic because even overexpression of wild type *CDH1* from *GAL1* promoter is almost lethal (Martinez et al, 2006). Furthermore, the survey did not directly address the importance of particular phosphorylation

sites. Here, I assessed the need for particular phosphorylation sites, in the context of endogenous expression levels, and elucidate the relationship between the number of phosphorylation sites, APC-Cdh1 activity, and the phenotype at the cellular level.

3.1. No single CDK phosphorylation site on Cdh1 is essential for viability

In order to assess the requirement for particular phosphorylation sites in the context of endogenous expression levels, Jonathan Robbins constructed a series of partially phosphorylatable CDH1 alleles (J. Robbins, PhD thesis). Serine of threonine residues in the CDK consensus motif were mutated to alanine, starting either with the most N-terminal or C-terminal site and mutating consecutive sites (J. Robbins, PhD thesis).

In the series of mutants where sites were mutated from the C terminus, mutation of up to eight phosphorylation sites caused no loss of viability (figure 3.1, blue line on the diagram). In contrast, mutants in N-terminal sites were more sensitive; while 7 C-terminal sites were sufficient for complete viability, the mutant allele bearing only 4 C-terminal phosphorylation sites was lethal (figure 3.1, green line on the diagram).

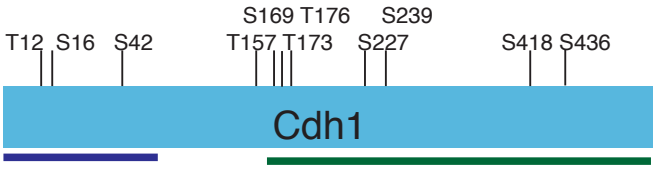

Figure 3.1: A scheme of Cdh1 with CDK consensus sites (S/T followed by a P residue). The sites are referred by their sequential number, counting from the most N-terminal site. The blue and green lines on the bottom indicate the minimal number of phosphorylation sites required for N-terminal and C-terminal sites, respectively (see text). These results are summarized from J. Robbins, PhD thesis.

Cell viability is therefore not dependent on any particular phosphorylation site, since alleles compatible with viability were constructed with two non-overlapping sets of phosphorylation sites; however, fewer sites are sufficient for viability on the N-terminal side, suggesting that N-terminal sites are have stronger effects on Cdh1 inhibition.

3.2. No single CDK phosphorylation site on Cdh1 is sufficient for viability

Follow up on this result, I asked whether any particular phosphorylation site might alone be sufficient for viability. Since only three most N-terminal phosphorylation sites were sufficient for viability, I reasoned that these sites might contribute the most, and are therefore the most likely candidates for phosphorylation sites sufficient for viability. Since overexpression of the inhibitor Acm1 from a galactose-inducible promoter (*GAL-ACM1*) was previously shown to allow for normal growth of *CDH1-m11* cells, these *CDH1* phosphomutants were constructed in *GAL-ACM1* background. Cells were then plated on glucose (*GAL-ACM1* off) to assess their viability.

Here, I will refer to the phosphorylation sites by the sequential number of the site from the N-terminus, and refer to the mutants by the phosphorylation sites that

are present (for instance, Cdh1-3P contains only the third phosphorylation site, but lacks the remaining sites).

I constructed partially phosphorylatable *CDH1* mutants bearing only the first, second or third phosphorylation site, as exact gene replacements to ensure endogenous expression levels. Upon plating onto glucose, none of these single phosphorylatable *CDH1* alleles allowed cell viability, since cells were not able to form colonies up on glucose (figure 3.2).

In addition, I constructed partially phosphorylatable alleles bearing combinations of two among the three N-terminal phosphorylation sites. I found that cells bearing the CDH1-2,3P allele (with the second and third sites present) were partially viable on glucose; however, compared to colony formation on galactose, colony formation was reduced by a factor of 10 to 100.

I conclude that among the phosphorylation sites in the N-terminal part, no single site was sufficient for viability, and that at least two phosphorylation sites are required for (partial) viability. Since I did not test the remaining 8 sites for sufficiency for viability, I cannot formally exclude that one of these sites might be alone sufficient for viability; however, this conclusion is justified by the fact that C-terminal sites appear weaker than the C-terminal sites in the ability to inhibit Cdh1.

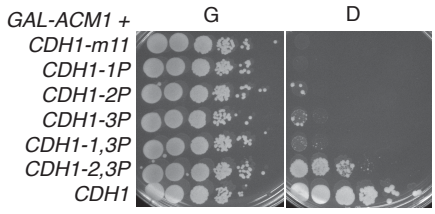

Figure 3.2: No single phosphorylation site is sufficient for viability. Tenfold dilutions of strains bearing *CDH1* alleles with only one or two phosphorylation sites. D, glucose; G, galactose.

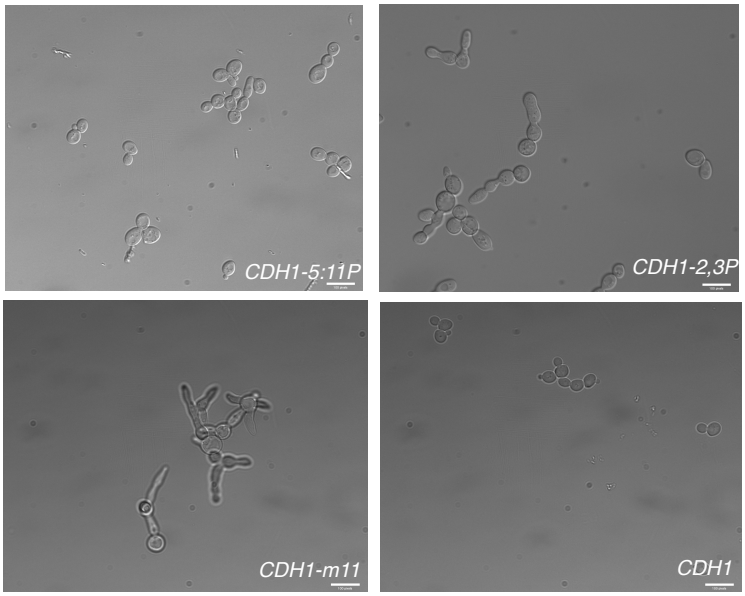

Figure 3.3: DIC images of cells bearing partially phosphorylatable *CDH1* alleles. Images were taken with 63x objective.

3.3. Cells with partially phosphorylatable *CDH1* alleles exhibit stochastic morphological abnormalities

To assess the phenotype of cells bearing partially phosphorylatable *CDH1* alleles, I took DIC images of cells in liquid cultures in glucose media. Cells bearing the unphosphorylatable *CDH1-m11* allele exhibited uniformly abnormal morphology (figure 3.3). These cells formed extremely elongated buds, owing to the inability to depolarize bud growth due to lack of mitotic Clb-CDK activity (Lew and Reed, 1993), and frequently rebudded multiple times (Robbins & Cross, 2010a).

In cultures of *CDH1-2,3P* cells, the long-budded or multiple budded cells represented the majority; however, a small fraction of normally budded cells were also observed. Other partially phosphorylatable *CDH1* mutants also showed sporadic morphologically defective cell cycles (Jonathan Robbins, PhD thesis). In particular, cells bearing *CDH1-5:11P* (originally named *CDH1-4N*; in this work the mutant is renamed for consistency with the naming used here), which lacks the 4 N-terminal sites, but has the remaining 7 C-terminal sites, were occasionally also long-budded, but the fraction of these morphologically abnormal cells was smaller than *CDH1-2,3P* cells.

3.4. Partially penetrant phenotype of *CDH1-2,3P*

To further characterize the phenotype in these cells lacking full phosphorylation control, I performed fluorescent time-lapse microscopy using strains with a bud neck marker, Myo1-mCherry, and the APC-Cdh1 biosensor (see chapter 2). In particular, I focused on the *CDH1-2,3P* mutant, which showed variability in cell morphology. The nuclear localization of the biosensor allowed me to monitor nuclear morphology and assess nuclear division. The cells were grown in a microfluidic chamber where I was able to rapidly switch media and induce or repress gene expression (see materials and methods). First, the cells were grown in galactose (*GAL-ACM1* on) to form a small microcolony of ~10 cells, and then switched to glucose to expose the phenotype of the *CDH1* allele. Acm1 is very rapidly degraded during mitotic exit and in G1 phase, and is stabilized by phosphorylation from budding to mitosis (Enquist-Newman et al, 2008). Therefore, the cells that have budded by the time a switch to glucose occurred were be protected until the next G1, but enter the next cell cycle with no leftover Acm1, as the depletion of *GAL-ACM1* has been shown to be very effective (Robbins and Cross, 2010a). I therefore count the first cell cycle in the experiment as the first cycle that the cell initiated as an unbudded cell in glucose.

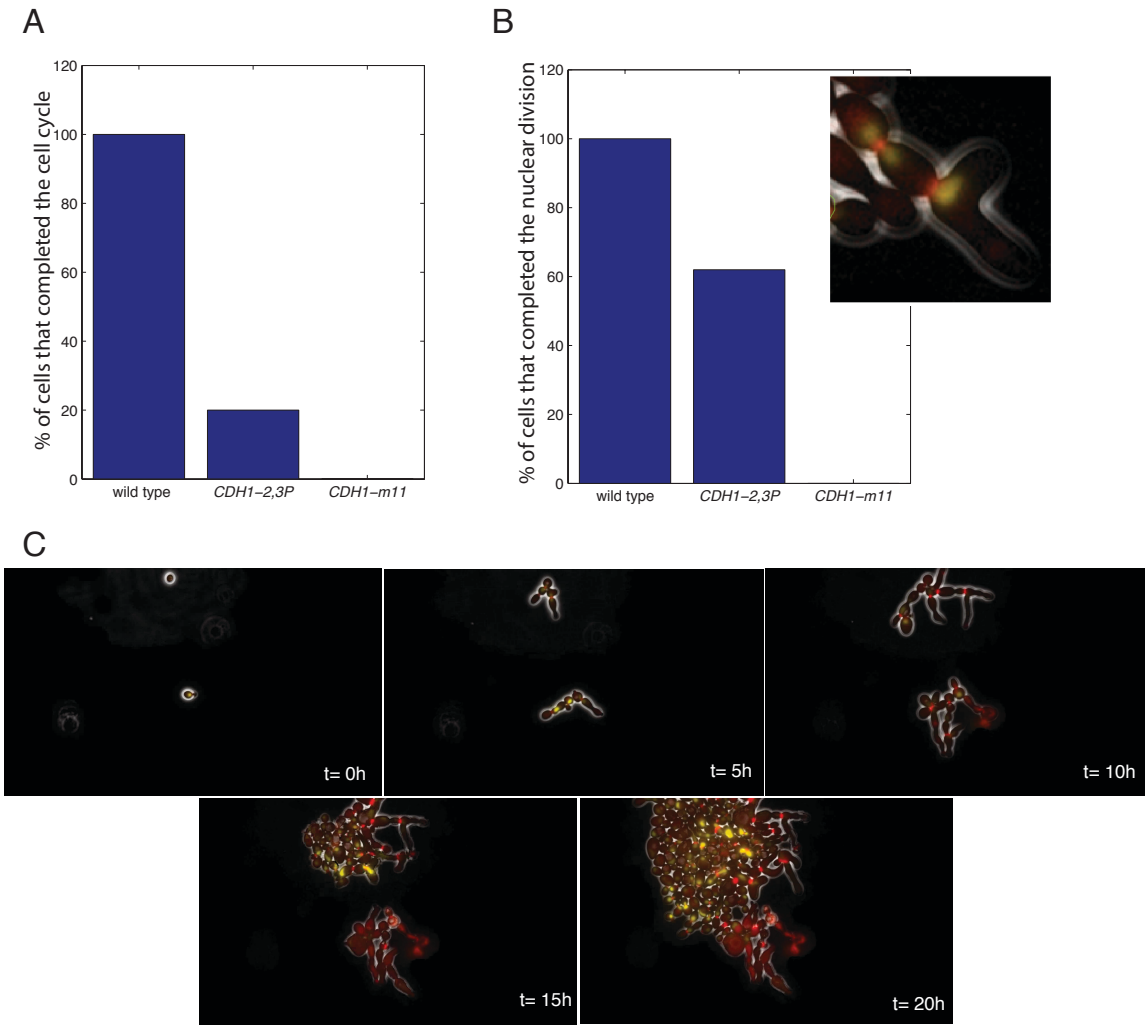

Figure 3.4: CDH1-2,3P mutant exhibits a partially penetrant cell cycle phenotype. A) Fraction of cells that completed the first cell cycle (starting as an unbudded cell in glucose). B) Fraction of cells that completed at least one nuclear division during the time-lapse. Inset, a composite image of a CDH1-2,3P cell that formed elongated buds and also completed the nuclear division. Red, Myo1-mCherry (bud neck marker); yellow, APC-Cdh1 biosensor (nuclear marker). C) Images at representative intervals from a 20-hour time-lapse of CDH1-2,3P cells illustrate partial penetrance in colony formation of CDH1-2,3P. Same fluorescent markers as in B.

CDH1-m11 cells uniformly arrested in the first cell cycle upon switch to glucose (figure 3.4). In accordance with previous results (Robbins and Cross, 2010a), these cells established a new bud site and proceeded to grow elongated buds without switching to isotropic bud growth, and never underwent cytokinesis (Myo1-mCherry signal remained present at the bud site). During the duration of the time lapse (7 hours), these cells often rebudded (i.e. established a new bud site either on the cell body or on the bud) and formed multiple elongated buds. The nuclei, marked by the localization of the biosensor, were stuck at the bud site, and remained undivided in all observed cells throughout the duration of the time-lapse (figure 3.4).

In contrast, *CDH1-2,3P* cells were variable. 20% of the cells (4/20) successfully completed the first cell cycle after switch to glucose (figure 3.4 A). Other cells formed elongated buds and rebudded, like *CDH1-m11* cells, without completing cytokinesis. I also observed variability in nuclear morphology in these cells. Frequently, nuclei rapidly migrated along the nascent buds. In addition, 62% (13/21) of arrested *CDH1-2,3P* cells performed at least one round of nuclear division (figure 3.4 B). However, I note that these nuclear divisions were often visibly aberrant – the nuclear mass separated unevenly, and the newborn nuclei remained attached. Nuclear divisions also occurred at very variable times throughout the arrest (shown on traces in figure 3.5), although due to

morphological abnormalities the precise timing of nuclear divisions was often impossible to score.

In summary, on the single cell level, *CDH1-2,3P* exhibited partially penetrant cell cycle phenotype, as a fraction of cells were capable of progressing through the cell cycle, and a fraction of cells arresting. While I label these cells “arrested” because of their morphological abnormality and failure to perform an essential cell cycle event (cytokinesis), these cells continued to perform other cell cycle events such as nuclear division and establishment of bud sites, and as judged by the growth on the colonies on the plates, at least some of these cells were ultimately viable.

It was surprising that a big fraction of *CDH1-2,3P* cells resembled arrested *CDH1-m11* cells, but still a fraction of these cells managed to escape and form colonies on glucose plates (figure 3.2). To investigate this phenomenon, I performed longer time-lapse experiments. In these experiments, single cells were plated in the microfluidic device, immediately switched to glucose media, and imaged for 20 hours. As described above, these cells grew elongated buds, re-budded, and divided their nuclei within that period. Strikingly, however, at 10 an 15 hours time points, some of these long-budded multinucleated cells started producing morphologically normal cells, and by the 20 hour time point, grew into a sizeable colony of mostly morphologically normal cells (figure 3.4 C), which

likely had the ability to form a macroscopic colony. This phenomenon was observed in 30% of imaged cells, while the rest of the cells did not recover and started to lyse by the end of the experiment.

However, in an attempt to investigate this phenomenon by recovering cells grown on glucose plates, I noticed that these cells were no longer able to arrest even transiently. I therefore conclude that the cells that switched to morphologically normal cells likely suffered an irreversible genetic change.

3.5. Complex phenotype of *CDH1-2,3P* due to partially regulated APC-Cdh1 activity

The APC-Cdh1 biosensor in these cells allowed me to assess the dynamics of APC-Cdh1 activity. *CDH1-m11* cells arrested with low fluorescence levels, suggesting persistently high APC-Cdh1 activity (figure 3.5 B). In contrast, arrested *CDH1-2,3P* maintained intermediate biosensor levels between wild type and *CDH1-m11* cells (quantified as average biosensor fluorescence in the mother cell body excluding the elongated bud, figure 3.5 B).

In addition, *CDH1-2,3P* cells exhibited dynamic biosensor levels in the arrest. This dynamics can at least partially be explained by mean fluorescence of the

cell dropping due to nuclear division as described in chapter 2.4. In addition, many *CDH1-2,3P* cells exhibited aberrant nuclear migration along the elongated buds. However, even in cells where the nucleus remained in the mother cell body (not in the bud) throughout the imaging period, the oscillations occurred without any nuclear division (figure 3.4 A). This implies APC-Cdh1 activity in *CDH1-2,3P* cells undergoes oscillations in activity, presumably due to cycles of phosphorylation and dephosphorylation of Cdh1-2,3P at the remaining two sites. This dynamic behavior was irregular in both amplitude and timing, and the time between peaks was generally longer than in wild type.

Overall, the results indicate that partial phosphorylation of Cdh1 allows for partial, but not complete inactivation of APC-Cdh1. Comparison with *CDH1-m11* reveals that Cdh1-2,3P allows for partial inactivation of APC-Cdh1, which implies that the remaining two phosphorylation sites are phosphorylated at least some of the time. However, due to dynamic activity of APC-Cdh1 in these arrested cells, precise quantification of APC-Cdh1 activity, compared to wild type APC-Cdh1 activity, was not possible.

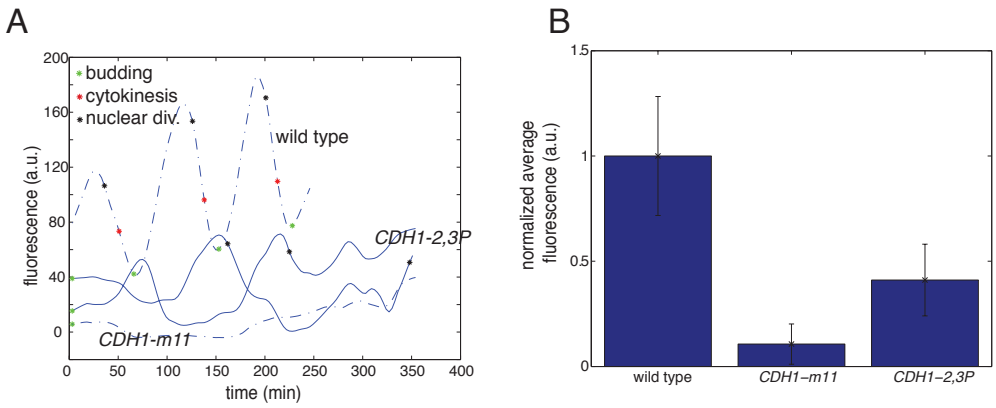

Figure 3.5: APC-Cdh1 activity in *CDH1-2,3P* cells. A) Representative time courses of APC-Cdh1 biosensor fluorescence for two *CDH1-2,3P* cells (solid lines), along with wild type and *CDH1-m11* cells (dashed lines). B) Quantification of average biosensor fluorescence intensities. Error bars represent standard deviation. Fluorescence intensities were corrected for autofluorescence by subtracting fluorescence intensities of unlabeled cells.

3.6. *CDH1-2,3P* cells arrest with dynamic Clb2 levels

I assessed whether partial phosphorylation of Cdh1 allows for accumulation of mitotic cyclin Clb2. *CDH1-m11* cells did not have any detectable Clb2 levels by western blot (figure 3.7), consistent with previous results (Robbins and Cross, 2010a). However, Clb2 was detected in *CDH1-2,3P* cells, although the level was lower than asynchronous wild type cells (figure 3.7).

To assess the Clb2 levels in *CDH1-2,3P* cells on the single cell level, I performed time-lapse microscopy using GFP-tagged endogenously expressed *CLB2* (Lu and Cross, 2010). In *CDH1-m11* cells, no detectable Clb2-GFP signal was observed. In contrast, in *CDH1-2,3P* cells, detectable Clb2-GFP accumulation was observed. Clb2-GFP levels were dynamic, and ranging from zero to approximately peak levels of wild type cells. Qualitatively, these traces were similar to APC-Cdh1 biosensor in *CDH1-2,3P* cells, with no regular pattern of oscillations.

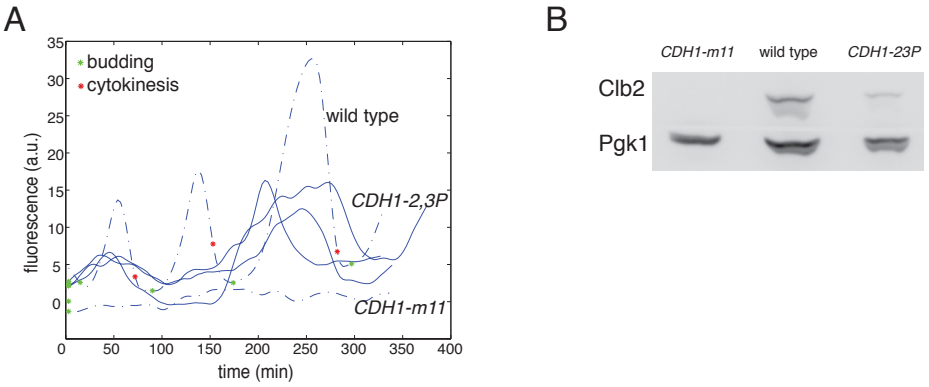

Figure 3.6: Clb2 levels in *CDH1-2,3P* cells. A) representative time courses of Clb2-GFP fluorescence in two *CDH1-2,3P* cells (solid lines), along with wild type and *CDH1-m11* cells (dashed lines). Fluorescence intensities were corrected for autofluorescence by subtracting fluorescence intensities of unlabeled cells. B) Immunoblots against Clb2 at 6 hours after switch to glucose (*GAL-ACM1* off).

3.7. Restoring Clb2 levels by introducing a partially degradation-immune *CLB2* allele does not rescue the cell cycle phenotype of *CDH1-2,3P*

Next, I wanted to test whether the levels of mitotic cyclin accumulated in *CDH1-2,3P* cells are sufficient for cell cycle progression (implying that other APC-Cdh1 targets are the limiting factor), or whether the cell cycle arrest occurs due to insufficient Clb2 levels. To do that, I introduced *CLB2-ken*, a partially non-degradable version of Clb2 expressed from the endogenous *CLB2* promoter instead of wild type *CLB2*, into *CDH1-2,3P* cells. Previously, it was found that the defects in entering into mitosis in *CDH1-m11* cells were due to inability to establish mitotic Clb-CDK activity, as introducing a completely non-degradable CLB2-kd allele into CDH1-m11 cells restored the depolarization of bud growth, and allowed for formation of mitotic spindle (Robbins and Cross, 2010a).

Clb2-ken is partially immune to degradation by APC; mutation of KEN boxes prevents degradation by APC-Cdh1, but not APC-Cdc20 (Wasch and Cross, 2002). I used only a partially degradation immune *CLB2-ken* with an expectation that I might be able to observe a complete rescue of cell progression; while using *CLB2-kd* restores even higher Clb2 accumulation, it does not allow for mitotic exit and results in arrest, which would make the interpretation of the result more difficult.

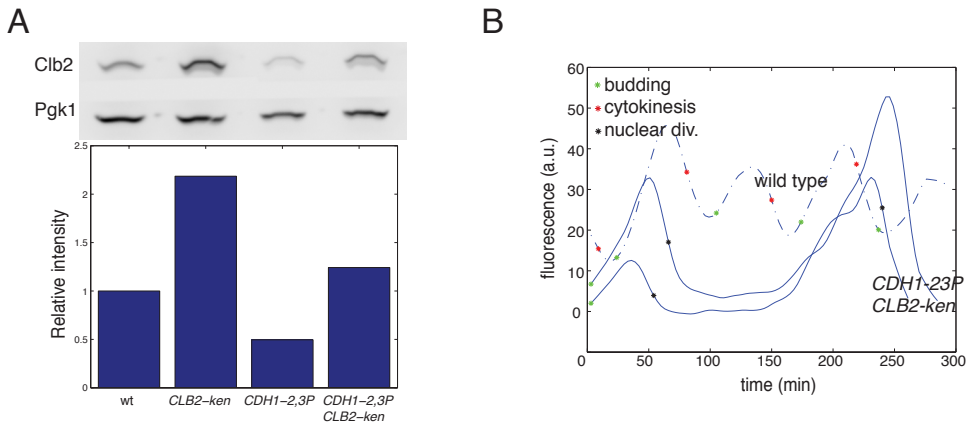

Figure 3.7: Restoring Clb2 levels does not rescue the phenotype associated with incomplete APC-Cdh1 inactivation. A) Immunoblots against Clb2 (top). Relative intensities of Clb2/Pgk1 signal, normalized to the wild type ratio (bottom). B) Representative time courses of the APC-Cdh1 biosensor fluorescence in two *CDH1-2,3P CLB2-ken* double mutant cells (solid lines) along with a wild type cell (dashed line). Fluorescence intensities were corrected for autofluorescence by subtracting fluorescence intensity of unlabeled cells.

CLB2-ken cells are viable and largely morphologically normal, but they contain approximately twice the amount of wild type Clb2 levels in asynchronous population (figure 3.7 A). Introducing *CLB2-ken* into *CDH1-2,3P* cells restored average Clb2 levels, measured by western blot, to about wild-type levels, but not to the levels of *CLB2-ken* cells (figure 3.7 B). This indicates that perhaps Clb2-ken can still be degraded by APC-Cdh1-2,3P, or that Clb2-ken degradation by APC-Cdc20 is higher in *CDH1-2,3P CLB2-ken* cells than in *CLB2-ken* cells (Clb2-ken is immune only to degradation by APC-Cdh1 and not to degradation of APC-Cdc20).

However, despite elevated Clb2 levels in these cells compared to *CDH1-2,3P* cells, the morphology and cell cycle progression phenotype of these cells remained similar to *CDH1-2,3P* cells. Time lapse microscopy of *CDH1-2,3P CLB2-ken* cells revealed no detectable difference from *CDH1-2,3P* cells. *CDH1-2,3P CLB2-ken* cells also displayed a variability in cell cycle progression, with a fraction of cells completing the first cell cycle after *GAL-ACM1* off switch (2/18 cells, compared to 4/20 for *CDH1-2,3P* cells). Occasional nuclear divisions in *CDH1-2,3P CLB2-ken* cells were also observed (8/20, compared to 13/21 for *CDH1-2,3P* cells). In arrested cells, the averaged levels of the APC-Cdh1 biosensor were similar to *CDH1-2,3P* cells, and the behavior of the biosensor was similarly dynamic (figure 3.7).

Overall, introducing partially non-degradable Clb2 into *CDH1-2,3P* cells did not rescue the phenotypes associated with the *CDH1-2,3P* mutant. Therefore, Clb2 is might not be the limiting target of APC-Cdh1-2,3P degradation in depolarizing bud growth and progression through the cell cycle. This contrasts with previous result, where rescue of the depolarized bud growth was achieved by introducing a completely non-degradable Clb2-kd into completely unregulatable *CDH1-m11* cells. A likely possibility is that Clb2-ken into cells does not cause establishment of Clb2-CDK activity with proper timing, even though the overall Clb2 levels are elevated. Using a GFP-tagged version of *CLB2-ken* in *CDH1-2,3P* cells would allow to directly assess the dynamics of Clb2-ken accumulation.

3.8. Periodic gene expression in *CDH1* phosphomutants

Periodic gene expression is associated with the cell cycle; in each cell cycle, a significant fraction of the genome undergoes once per cell cycle activation of expression (Spellman et al, 1998). However, the relationship between cell cycle regulators and periodic gene expression is not fully understood, and it remains unresolved whether, and to what extent, these changes in gene expression are regulated by cyclin-CDK activity and whether periodic gene expression is sustained in arrested cells at various cell cycle stages (Orlando et al, 2008;

Simmons-Kovacs et al, 2011; Bristow et al, 2014; see also chapter 5). Here, I wanted to assess whether lack of inhibition of APC-Cdh1 still allows for expression of cell cycle-regulated genes.

To address these questions, I measured expression of three genes, associated with the three main gene expression regulons in the yeast cell cycle, in *CDH1-m11* and *CDH1-2,3P* cells. This was done using constructs where a fluorescent protein was placed under the control of the gene promoter. CLN2 is a representative of the regulon associated with the transcription at the G1/S phase border; it is regulated by transcriptional factors SBF and MBF. *CLB2* promoter is a representative of the G2/M regulon, and its transcription is regulated by a complex containing Mcm1, Fkh1/Fkh2 and Ndd1 (Koranda et al, 2000). *SIC1* promoter is a representative of the regulon expressed at the exit of mitosis (G2/M border), which is regulated by transcription factors Swi5 and Ace1 (see introduction).

CLN2 promoter was turned on in both *CDH1-m11* and *CDH1-2,3P* cells (figure 3.8); the *CLN2*pr-GFP signal was similar to wild type cells and possibly periodic, although the oscillations were not as regular as in wild type cells. This was expected, given the fact that *CLN2* is expressed before APC-Cdh1 inactivation and APC-Cdh1 inactivation does not have a role in preventing the transcription of G1/S genes. It is also consistent with the observations of elongated bud

morphology and periodic rebudding in *CDH1-2,3P* and *CDH1-m11* cells, since Cln-CDK is the driver of polarized bud growth and rebudding (Lew and Reed, 1993).

CLB2 promoter was not activated in *CDH1-m11* cells (figure 3.8). This is in agreement with the proposed positive feedback model for mitotic cyclin expression, in which Clb2-CDK activity is required for full induction of *CLB2* expression (Amon et al, 1993). This establishes that inactivation of APC-Cdh1 is essential not only for accumulation of Clb2 protein, but also for activation of *CLB2* expression (see chapter 2).

In contrast, *CLB2* promoter was activated in *CDH1-2,3P* cells. The *CLB2*pr-GFP signal was as high as in wild type cell peaks, with no regular periodic activity, implying that *CLB2* promoter might be permanently turned on, although I note that due to very low dynamic range of *CLB2*pr-GFP, low signal to noise ratio makes it challenging to establish whether the dynamics is due to periodic activation or merely due to noise.

Similar results were observed for *SIC1* promoter; *CDH1-m11* cells did not activate *SIC1* transcription, while *CDH1-2,3P* cells turned on expression of *SIC1* promoter (figure 3.8).

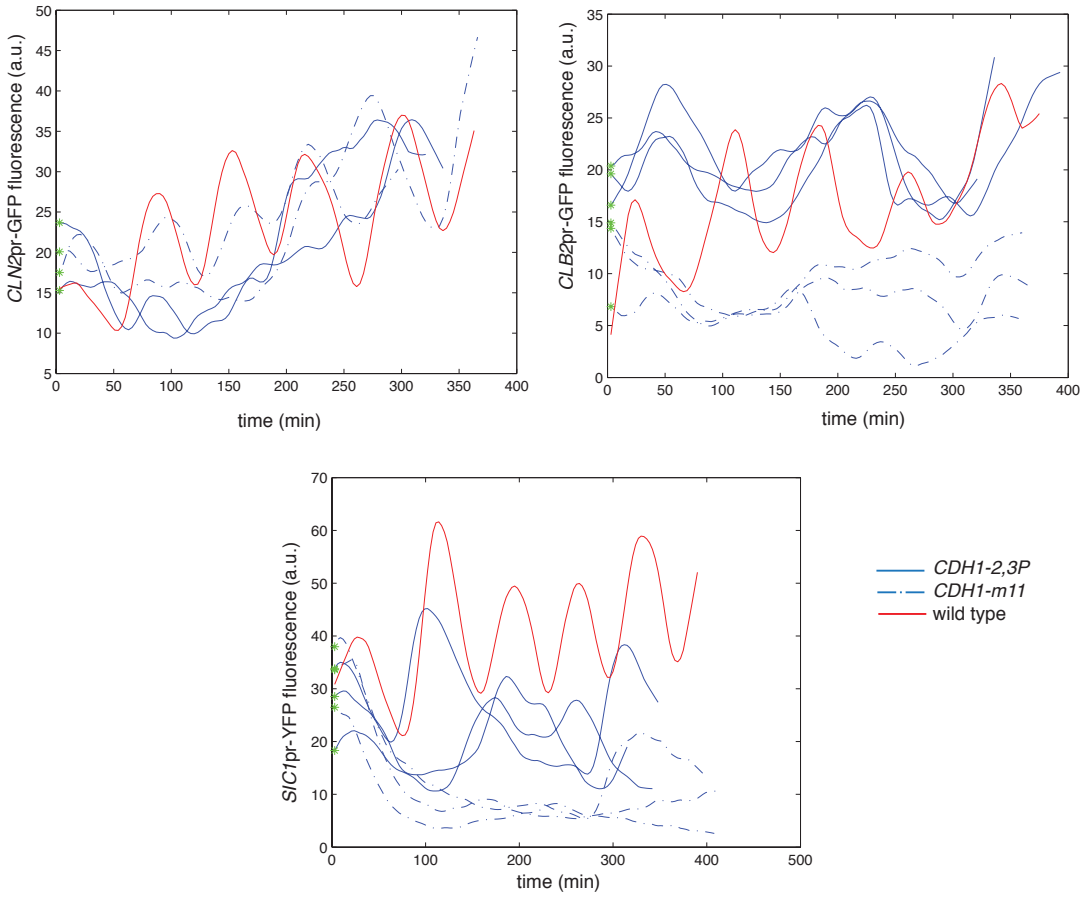

Figure 3.8: Cell cycle-associated transcription in *CDH1* phosphomutants. Upper left, expression of *CLN2*pr-GFP. Upper right, expression of *CLB2*pr-GFP. Bottom, expression of *SIC1*pr-YFP. Fluorescence intensities were corrected for autofluorescence by subtracting fluorescence intensities of unlabeled cells.

In conclusion, APC-Cdh1 inactivation is required for activation of cell cycle-regulated promoters. This set of experiments is relevant for the work presented in chapter 5, where I, in collaboration with S. Jamal Rahi and Kresti Pecani, analyzed cell cycle-regulated gene expression in absence of B-type cyclins. Since unrestrained activity of APC-Cdh1 prevents accumulation of mitotic cyclins, this experiment is similar, although not exactly equivalent, to the experiment performed in chapter 5, where all B-type cyclins *CLB1-6* were genetically deleted. The differences are that Clb5 and 6 are present in *CDH1-m11* cells (and not in *clb1-6* cells), but APC-Cdh1-m11 also does not allow for accumulation of other APC-Cdh1 targets that might in principle be present in *clb1-6* cells. Generally, later cell cycle genes are largely not expressed in cells deleted for B-type cyclins (see chapter 5), although *SIC1* was found to be a notable exception of a gene that is expressed in clb deleted cells (Rahi et al, submitted). Lack of expression of *SIC1* in *CDH1-m11* cells suggests that B-type cyclin-CDK-independent mechanism of *SIC1* expression is dependent on one (or more) of the APC-Cdh1 targets; or that presence of Clb5 and 6 (or perhaps residual Clb1-4 not fully degraded by APC-Cdh1-m11) inhibits *SIC1* expression. Global transcriptome profiling in *CDH1-m11* cells would provide an insight into a complete picture of gene expression and, in comparison to the data from cln-clb-cells (Chapter 5) reveal if inactivation of APC-Cdh1 is required for the periodic gene expression.

However, in partially phosphorylatable *CDH1-2,3P* cells, I found that expression of cell cycle-regulated genes (at least for the representatives of the two regulons) was allowed. This suggests that partial restrainment of APC-Cdh1 activity, while not sufficient for cell cycle progression (these cells were arrested as long-budded cells), was sufficient for continuation of the cell cycle transcriptional program.

3.9. Conclusions and future directions

In this study, I followed up on previous work addressing multisite phosphorylation of Cdh1. Previous studies have partially addressed this question; Zachariae et al found that the association with the core APC depends gradually on the number of phosphorylation sites on Cdh1 (Zachariae et al, 1998). Previous data also showed that no single site on Cdh1 is necessary for viability, but that some sites contribute more to the inhibition, as concluded from the number of sites required. (J. Robbins, PhD thesis). Here, I expanded these findings by defining a minimal set of phosphorylation sites required, and an in-depth analysis of the phenotype associated with partial removal of phosphorylation sites.

First, I tested whether one single site might be sufficient for viability. Of the three more likely candidates among the N-terminal sites, no single site mutant was viable. Therefore, no single site is sufficient for required inactivation of APC-Cdh1. However, it is formally possible, although unlikely, that any of the weaker C-terminal sites might be sufficient for viability. Overall, this screen for partially phosphorylatable *CDH1* mutants has an implication for the mechanism of Cdh1 phosphorylation, which could be addressed by carrying out biochemical experiments.

An important observation is that the failure of sufficient inactivation of APC-Cdh1 in these mutants is stochastic, not deterministic. Rather that a uniform response of in the entire population of cells, two partially phosphorylatable mutants were found (*CDH1-2,3P* and *CDH1-5:11P*) that exhibit variability in cell morphology. The frequency of morphologically normal and arrested cells was different in those two mutants, implying that degree of APC-Cdh1 inactivation might modulate the probability of successful cell cycle progression. On the single cell level, time-lapse microscopy of *CDH1-2,3P* cells showed that while the majority of the cells were unable to progress through the cell cycle, a small fraction of cells completed the cell cycle.

The phenomenon, in which genetically identical cells exhibit variability in phenotype, is called partial penetrance. Partial penetrance has been observed

and characterized in many biological systems, including sporulation in Bacillus subtilis (Eldar et al, 2009) and vulval development in Caenorhabditis elegans (Milloz et al, 2008), but it has not been well studied in budding yeast cell cycle, although mutants that cause stochastic cell cycle arrest have been identified (for instance, stochastic G1 arrest in *cln1,2* cells (Skotheim et al, 2008)). It is generally believed that partial penetrance in genetically identical cells is caused by molecular noise.

Interestingly, *CDH1-2,3P* also exhibited partial penetrance in long-term growth and colony formation. Consistent with partial ability to form colonies on agar plates, time lapse imaging of single CDH1-2,3P cells revealed that even though all cells initially become long-budded, resembling a *CDH1-m11*-like arrest, a fraction of cells escaped arrest and gave rise to normally dividing progeny.

Using the quantitative essay for APC-Cdh1 activity in partially phosphorylatable *CDH1* mutants, I aimed to further characterize the stochastic cell fate in *CDH1-2,3P* cells. For instance, by correlating cell cycle progression with APC-Cdh1 activity in single cells, one might be able to discriminate whether the variability is caused upstream or downstream of Cdh1 inactivation; if the degree of APC-Cdh1 inactivation as measured by biosensor correlates with probability of cell cycle completion, the cause is likely in upstream regulators, whereas if APC-Cdh1 is inactivated to a (on average) uniform level in both arrested and

unarrested cells, one might conclude that probability of cell cycle progression is determined by the molecular noise downstream of Cdh1 phosphorylation.

However, this experiment was hindered by the technical limitations of the biosensor. Quantification of APC-Cdh1 activity in single *CDH1-2,3P* cells was impossible because of dynamic behavior of the system. By comparison to *CDH1-m11* cells, an indisputable conclusion is that APC-Cdh1-2,3P is partially inactivated, which implies that Cdh1-2,3P is phosphorylated at the remaining two sites at least some of the time; however, I cannot make further quantitative statements about APC-Cdh1 activity.

To improve this assay, one would need to devise an experimental system where partially phosphorylatable Cdh1-2,3P would be “locked” in a phosphorylated state and eliminate APC-Cdh1-independent degradation of the biosensor. Since Cdc14 is responsible for dephosphorylation of Cdh1, the assay would require deleting *CDC14* to maintain the phosphorylation state of Cdh1-2,3P. This would presumably lock the cells with partial APC-Cdh1 activity corresponding to fully phosphorylated Cdh1-2,3P; however, this experimental setup would have other limitations. Because *CDC14* is essential for mitotic exit, deletion of *CDC14* would by itself interfere with cell cycle progression. The experiment could in principle be done with a temperature-sensitive *cdc14* allele.

Partial penetrance observed in *CDH1-2,3P* is in dramatic contrast with the stereotyped inactivation of APC-Cdh1 with highly regular timing in wild type cells (chapter 2). This highly regular timing in wild type suggests an evolved mechanism for noise buffering and minimizing variability. Partial removal of a subset of phosphorylation sites greatly increased cell-to-cell variability. However, this variability is not in timing of APC-Cdh1 inactivation, but rather, depending on the two possibilities above, the degree of APC-Cdh1 inactivation, or the degree by which partially inactivated APC-Cdh1 can allow for cell cycle progression.

It therefore remains unresolved how the partially penetrant phenotypes in cells with partially phosphorylatable *CDH1* arise. To gain understanding of these phenotypes, I asked how multiple regulatory mechanisms contribute to APC-Cdh1 inactivation and interact with each other in the next chapter.

Chapter 4: Exploring the interactions between APC-Cdh1 regulators

Multiple negative regulators of APC-Cdh1 inactivation exist (see introduction). While preventing binding of Cdh1 to the APC core by means of inhibitory phosphorylation of Cdh1 by CDK is the most important mechanism (Zachariae et al, 1998), there are other additional mechanisms. APC-Cdh1 is inhibited by a pseudosubstrate inhibitor Acm1 (Martinez et at, 2006), and Cdh1 is also regulated by nuclear export, mediated by a karyopherin Msn5 (Jaquenoud et al, 2002). Furthermore, multiple cyclins, associated with CDK, can potentially have a role in Cdh1 phosphorylation. Initial work has suggested G1 cyclins to be essential for Cdh1 inactivation (Amon et al, 1993), but subsequent work has implied direct roles of Clb3,4 and 5 (Yeong et al, 2001), and Clb5,6 (Huang et al, 2001), in regulation of Cdh1. In this chapter, I explore the contribution of and the interplay between these multiple redundant regulatory mechanisms.

In addition to CDK, Cdh1 was found to be phosphorylated at multiple other sites by additional kinases (Hall et al, 2006), although significance of this phosphorylation is not understood. In particular, phosphorylation of Cdh1 by the polo kinase Cdc5 was suggested to contribute to APC-Cdh1 inactivation (Crasta et al, 2008), although conclusions of those results were later disputed (Robbins

and Cross, 2010a). I do not address phosphorylation of Cdh1 by other kinases in this work.

4.1. Deletion of *CLB5* and *6* delays APC-Cdh1 inactivation

To assess the contribution of the S-phase cyclins to APC-Cdh1 inactivation, I performed time lapse experiments and measured the time of inactivation of APC-Cdh1 in *clb5,6* cells with respect to budding, using the APC-Cdh1 biosensor as described in chapter 2. I performed the described data analysis procedure to remove unreliable data points (chapter 2.5). I find that deletion of *CLB5* and *6* still allows for reliable APC-Cdh1 inactivation, as there were no morphological defects observed in *clb5,6* cells, and biosensor levels oscillated during the experiment. However, the apparent inactivation of APC-Cdh1 is delayed on average by 6 minutes with respect to wild type cells (measured with respect to budding; figure 4.1). While the difference is not big, it is statistically significant (Mann-Whitney $p=2.8*10^{-4}$), and probably biologically meaningful, since many cell cycle events occur on in short time in budding yeast. A delay of the same Ase1 degron fragment degradation has previously been observed qualitatively in bulk cultures (Huang et al, 2001).

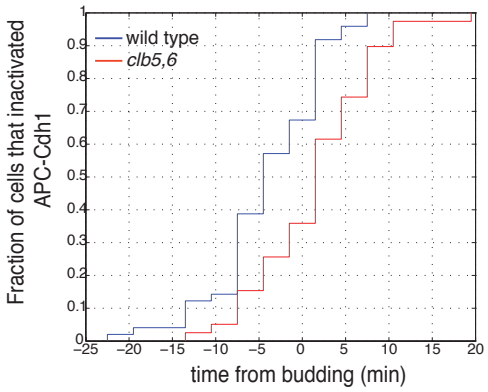

Figure 4.1: Timing of inactivation of APC-Cdh1 in *clb5,6* cells, measured by time-lapse microscopy with APC-Cdh1 biosensor.

This suggests that Clb5 and 6-CDK are probably the physiological kinases responsible for inactivating APC-Cdh1. However, clearly, other cyclin-CDKs and/or other regulators are capable of carrying out sufficient APC-Cdh1 inactivation, either later in the cell cycle, or with reduced efficiency.

4.2. Partially phosphorylatable *CDH1-2,3P* allele shows negative genetic interactions with *clb5* and *acm1*

Next, I looked for genetic interactions of deletions of APC-Cdh1 regulators with the partially phosphorylatable *CDH1* mutant, *CDH1-2,3P*. *CDH1-2,3P* cells are viable, but have a reduced ability to form colonies, and exhibit stochastic morphological phenotypes associated with incomplete inactivation of APC-Cdh1 (chapter 3). Again, the strains were constructed in *GAL-ACM1* background.

First, I tested interactions with *ACM1* and *MSN5* deletions. The logic of this experiment was that inhibition by Acm1 or nuclear export (via Msn5) might become essential if activity of APC-Cdh1 is not sufficiently restrained by Cdh1 phosphorylation. Furthermore, nuclear export by Msn5 might depend specifically on phosphorylation at particular sites on Cdh1.

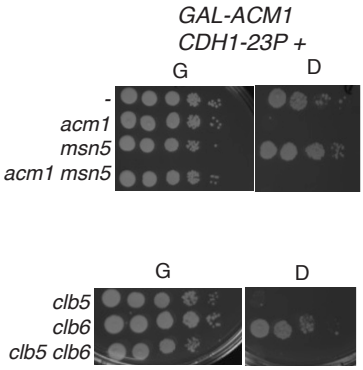

Figure 4.2: Genetic interactions with *CDH1-2,3P*. Top, genetic interactions with *acm1* and *msn5*. Bottom, genetic interactions with *clb5* and *clb6*. Strains were constructed in *GAL-ACM1* background. Tenfold serial dilutions were plated. G, galactose; D, glucose.

Deletion of *MSN5* and *ACM1* had no effects on viability and colony formation in wild-type *CDH1* cells (J. Robbins, PhD thesis; data not shown). *CDH1-2,3P* showed no genetic interaction with *msn5* on the level of colony formation. However, *CDH1-2,3P* was lethal in combination with deletion of *ACM1* (figure 4.2). This indicates that endogenous levels of Acm1 contribute to inhibition of APC-Cdh1, and that this inhibition becomes essential when APC-Cdh1 activity is not sufficiently restrained by phosphorylation.

For *MSN5*, genetic interactions with other partially phosphorylatable alleles have been tested before, and no genetic interactions on the level of colony formation were found with any of the tested partially phosphorylatable CDH1 mutants (J. Robbins, PhD thesis). Nuclear export mediated by Msn5 requires Cdh1 phosphorylation (Jaquenoud et al, 2002). The interpretation of this result can be that Msn5 does not physically interact with any particular phosphorylation site, such that nuclear export of Cdh1 can occur if regardless of the particular phosphorylation site. An alternative explanation is that the nuclear export has a minor contribution to APC-Cdh1 inactivation, and its elimination does not have a noticeable effect, at least on the level of colony formation.

Next, I tested genetic interactions of *CDH1-2,3P* with deletions of *CLB5* and *6*, which were found to likely be the main physiological kinase for Cdh1 phosphorylation (chapter 4.1). The idea behind this experiment was that if the

remaining Cdh1 sites are phosphorylated exclusively by Clb5 and/or Clb6-CDK, deletion of *CLB5* and/or *6* would phenocopy the completely unphosphorylatable *CDH1-m11* allele and result in loss of viability.

clb5,6 cells are fully viable and have no defects in colony formation (data not shown). I found that deletion of *CLB5* in *CDH1-2,3P* background resulted in loss of viability (figure 4.2). Deletion of *CLB6* did not have any effects, presumably because Clb6-CDK contributes significantly less to the total S-phase cyclin-CDK activity. This is probably due to the fact that it is about 10x less abundant than Clb5 (Cross et al, 2002), and generally deletion of *CLB6* has no phenotype if *CLB5* is present.

Similarly, deletion of *CLB5* also resulted in lethality in combination with the *CDH1:5:11P* mutant lacking the N-terminal phosphorylation sites (J. Robbins, PhD thesis). This result shows that when phosphorylation control is partially lost by removing either the N-terminal or the C-terminal sites, other cyclin-CDKs that are otherwise capable of compensating for loss of Clb5-CDK, are not sufficient for Cdh1 phosphorylation; however, alternative interpretations, involving indirect effects of Clb5-CDK phosphorylation of other targets, are possible. Because CDK phosphorylation causes stabilization of Acm1 (Melesse et al, 2014), it is possible that deletion of *CLB5* in partially phosphorlatable *CDH1* mutants causes lethality due to failure of Acm1 stabilization. If this interpretation is

correct, mutating phosphorylation sites on Acm1 would phenocopy loss of *CLB5* in partially phosphorylatable *CDH1* mutants.

4.3. Simultaneous deletion of *ACM1*, *CLB5* and *CLB6* causes stochastic morphological defects

Based on the results that Clb5-CDK is likely the physiological kinase responsible for Cdh1 phosphorylation, and that Acm1 becomes important if phosphorylation of Cdh1 is impaired, we reasoned that simultaneous loss of *CLB5*, *CLB6* and *ACM1* might by itself have deleterious consequences even in presence of all the phosphorylation sites on Cdh1.

The triple mutant cells were constructed in the GAL-ACM1 background and then plated onto glucose media to assess their viability. Cells with the triple deletion of clb5,6 acm1 were viable and able to form colonies on glucose (data not shown). However, a small fraction of these cells (10%) exhibited a morphological abnormality. Morphologically abnormal cells were not observed in either *acm1* or *clb5,6* cells. These cells had abnormally elongated buds. This phenotype was seen before in partially phosphorylatable mutants (chapter 3) and resembles the long-budded morphology of *CDH1-m11* cells. Hyperpolarized

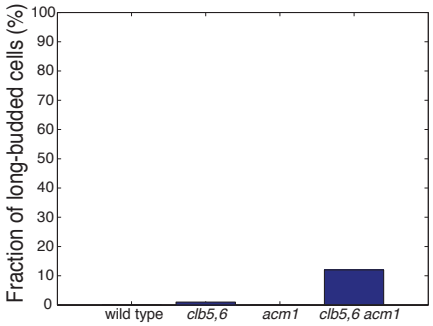

Figure 4.3: Stochastic morphological defects in *acm1 clb5,6* cells. Fraction of morphologically abnormal long budded cells.

growth is an indicator of lack of mitotic cyclin-CDK activity; mitotic cyclin-CDKs are required for the switch to isotropic bud growth (Lew and Reed, 1993). Therefore, presence of hyperpolarized buds in these cells could be an indicator of stochastic defects in APC-Cdh1 inactivation, similar as observed in partially phosphorylatable *CDH1* mutants (chapter 3). This interpretation is plausible because *ACM1* has so far not been found to have any other role than inhibition of APC-Cdh1; although other interpretations involving direct effects on mitotic cyclins of downstream targets that regulate the bud growth switch are also possible.

4.4. Deletion of G1 cyclins alleviates the stochastic defects in partially phosphorylatable *CDH1* mutants

Initially, G1 cyclins were implicated in APC-Cdh1 inactivation (Amon et al, 1993), although it was later suggested that they are not sufficient (Yeong et al, 2001). To clarify this, I examined genetic interactions between partially phosphorylatable *CDH1* alleles and deletions of *CLN1* and *2*. The logic behind this experiment was the same as the *CLB5,6* experiment; if Cln1 and 2-CDK were uniquely required for phosphorylation of the remaining Cdh1 sites, deletion

of *CLN1* and *2* in that background would phenocopy unphosphorylatable *CDH1-m11* and cause lethality.

The strains were constructed in *GAL-ACM1*, as well as *MET3-CLN2* background, in which *CLN2* is conditionally expressed in absence of methionine (but not expressed in + met) because deletion of *CLN1* and *2* is severely deleterious and results in frequent G1 arrest (Skotheim et al, 2008). The assays were then carried out on media with added methionine.

Surprisingly, unlike *CDH1-2,3P*, the triple mutant *CDH1-2,3P cln1,2* had no reduced ability to form colonies. This is apparent from the image in figure 4.4 A; however, to quantitatively assess the ability to form colonies, I plated bigger volumes of cultures to count colony-forming units. The ability to form colonies in the *CDH1-2,3P* mutant was decreased approximately tenfold (figure 4.4 B, bottom left, compare G+met with D+met (*MET3-CLN2* off in both cases)). In comparison, the ability to form colonies was restored in *CDH1-2,3P cln1,2* cells (figure 4.4 B, bottom right, D+met), although the colony number was still slightly reduced by approximately 40%. It can also be observed that turning on *MET3-CLN2* in *CDH1-2,3P* background, which causes moderate overexpression, as well as a shift in timing of expression, of G1 cyclins, further reduces the colony formation in *CDH1-2,3P* (figure 4.4 B, bottom left, D+met).

In liquid culture, *CDH1-2,3P* cells exhibited hyperpolarized buds, indicating failure in bud growth depolarization owing to only partial APC-Cdh1 inactivation, as described before (chapter 3.3). However, the triple mutant *CDH1-2,3P cln1,2* cells did not exhibit hyperpolarized but growth D+met (but were hyperpolarized in D-met where *MET3-CLN2* was on; figure 4.4 C). Therefore, the morphological defects caused by insufficient APC-Cdh1 inhibition were completely restored by deleting *CLN1* and *CLN2*. I also note that *CDH1-2,3P cln1,2* cells were, similarly to *cln1,2* cells, enlarged, owing to a well-studied prolonged growth period in G1 phase in absence of Cln1,2-CDK (Skotheim et al, 2008).

To assess the growth of these cells quantitatively, I performed time-lapse microscopy of these cells. The strains contained Myo1-mCherry, the bud neck marker, to measure the duration of the unbudded and budded periods of the cell cycle. As noted above, deletion of *CLN1* and *CLN2* causes extended G1 (Skotheim et al, 2008); both *cln1,2* cells, as well as *CDH1-2,3P cln1,2* cells, exhibited longer unbudded periods in both mothers and daughters compared to wild type (data not shown).

As described in chapter 3.4, only 20% of *CDH1-2,3P* cells completed the first cell cycle upon switching to glucose (and did so with a delay, compared to the distribution budding to cytokinesis times for wild type; figure 4.4 D); the remaining 80% of the cells were arrested as long-budded cells and did not

Figure 4.4: Genetic interactions between partially phosphorylatable *CDH1* mutants and deletion of *CLN1,2*. Abbreviations: D, glucose; G, galactose; Met, methionine. Strains were constructed in *GAL-ACM1 MET3-CLN2* background. A) Tenfold serial dilutions of indicated strains. B) Counts of colony forming units of indicated strains, normalized to number of colonies of each culture on G-met. Error bars are standard error of the mean between plating triplicates. C) Representative DIC images of cells with indicated genotypes in indicated media. Images were taken 6 hours after switch from G-Met. D) Duration of the budded period of the cell cycle measured by time lapse microscopy using Myo1-mCherry as a bud neck marker in D+Met. D) Fraction of unbudded (u), budded (b) and long budded (lb) cells of indicated genotype in D+Met.

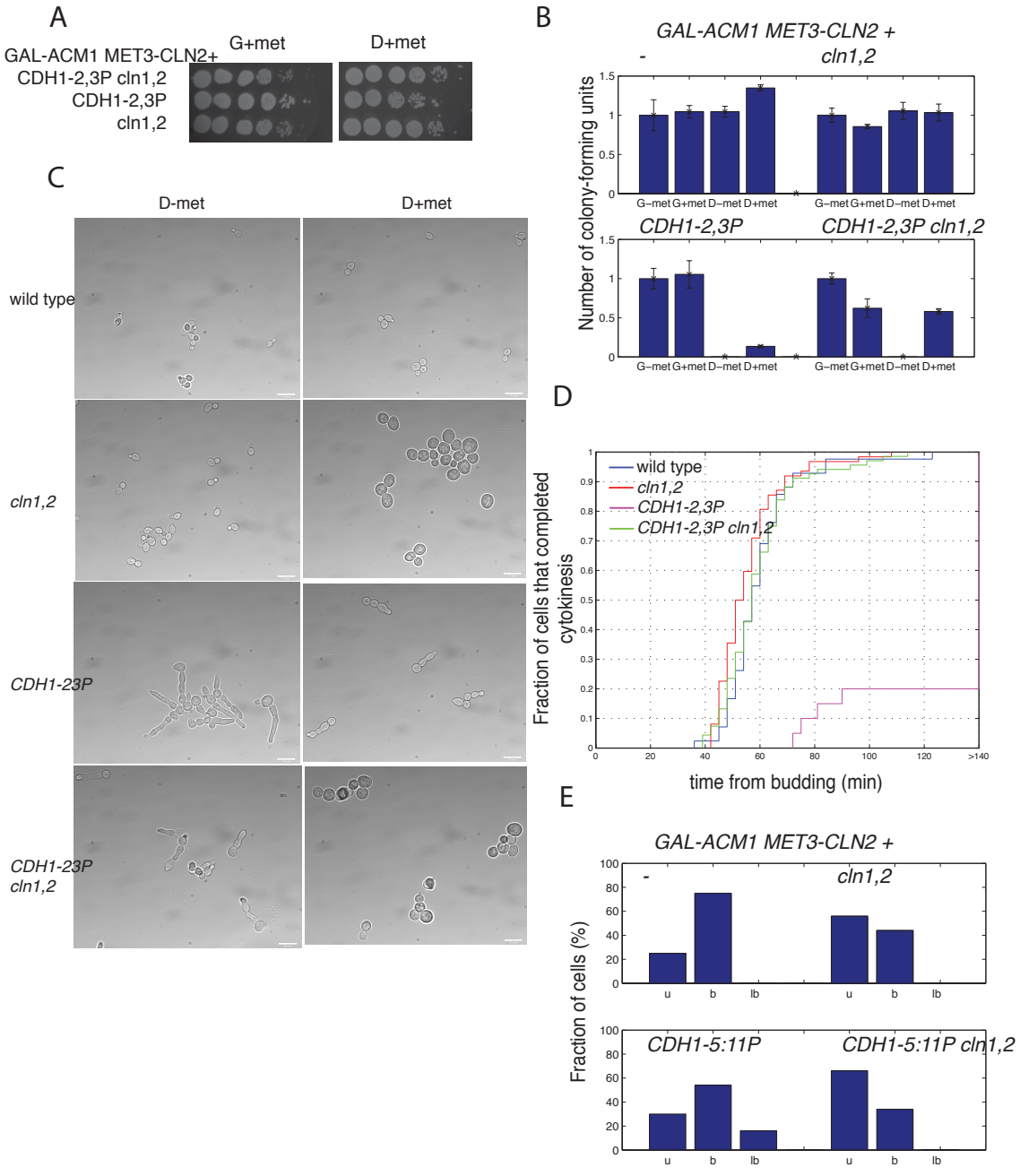
A
G+met
D+met
GAL-ACM1 MET3-CLN2+
CDH1-2,3P cln1,2
CDH1-2,3P
cln1,2
B
GAL-ACM1 MET3-CLN2 +
-
cln1,2
Number of colony-forming units
G−met G+met D−met D+met
CDH1-2,3P
CDH1-2,3P cln1,2
C
D-met
D+met
wild type
cln1,2
CDH1-23P
CDH1-23P
cln1,2
D
wild type
cln1,2
CDH1-2,3P
CDH1-2,3P cln1,2
Fraction of cells that completed cytokinesis
time from budding (min)
E
GAL-ACM1 MET3-CLN2 +
-
cln1,2
Fraction of cells (%)
u
b
lb
CDH1-5:11P
CDH1-5:11P cln1,2

complete cytokinesis (Myo1-mCherry marker remained at the bud site throughout). In contrast, 100% of *CDH1-2,3P cln1,2* cells completed cytokinesis, and did so with no delay in timing with respect to wild type or *cln1,2* cells (figure 4.4 D). Therefore, deletion of *cln1,2* in *CDH1-2,3P* background allows not only for depolarizing bud growth, but also for reliable cell cycle progression until cytokinesis.

Overall, no observed cell cycle defects in *CDH1-2,3P cln1,2* cells are therefore somewhat inconsistent with only partial inability to form colonies (figure 4.4 B). A reduced ability to form colonies could be due to occasional G1 arrests due to *cln1,2* deletion; however, no colony formation defects is observed for *cln1,2* cells on D+met. The likely explanation for this discrepancy is a systematic plating error in the experiment either for *CDH1-2,3P cln1,2* cells or *cln1,2* cells.

To test whether this rescue of partially phosphorylatable *CDH1* mutants is specific to the particular two phosphorylation sites present in the *CDH1-2,3P* mutant, I looked for genetic interactions of another partially phosphorylatable *CDH1* mutation that causes stochastic failures in APC-Cdh1 inactivation with *cln1,2* deletion. As above, these strains were constructed in *GAL-ACM1 MET3-CLN2* background. On glucose + methionine, cells bearing the *CDH1-5:11P* allele, which encodes Cdh1 protein that is missing the N-terminal 4 sites but have the 7 C-terminal sites (J. Robbins, PhD thesis), arrested as long-budded

cells with about 20% frequency (figure 4.4 E). However, these long budded cells were completely absent in *CDH1-5:11P cln1,2* strain (figure 4.4 E). I note that both *CDH1-2,3P cln1,2* and *cln1,2* strains had a bigger fraction of unbudded cells, owing to the prolonged G1 phase in absence of *CLN1* and *CLN2* (Skotheim et al, 2008).

In summary, deletion of G1 cyclins in strains bearing partially phosphorylatable *CDH1* alleles alleviates the phenotype of associated with incomplete APC-Cdh1 inactivation, and allows for both reliable bud growth depolarization, as well as timely cell cycle progression throughout the rest of the cell cycle. This result was unexpected and opposite to the prediction based on suggested role of Cln1,2-CDK in inhibitory phosphorylation of Cdh1.

4.5. Deletion of *CLN1,2* does not restore mitotic cyclin levels in partially phosphorylatable *CDH1* mutants

The morphological defects in cells bearing unphosphorylatable or partially phosphorylatable alleles have been traced to the inability to accumulate mitotic cyclins; mitotic cyclins are required for switching from polarized to depolarized bud growth (Lew and Reed, 1993), and in their absence, abnormally elongated

buds are formed. Introducing non-degradable Clb2 into *CDH1-m11* cells restored the ability to depolarize bud growth (Robbins and Cross, 2010a)

Based on these predictions, I reasoned that deletion of *CLN1* and *2* might, through one of many potential pathways, allow for accumulation of higher levels of mitotic cyclins in the *CDH1-2,3P* cells. To test that, I measured Clb2 levels by immunoblotting in asynchronous cultures 6 hours after switching to glucose media with methionine. As noted in chapter 3.6, *CDH1-2,3P* cells have reduced but detectable Clb2 levels. *cln1,2* cells have approximately wild-type levels of Clb2. However, Clb2 levels in the triple mutant *CDH1-2,3P cln1,2* are only comparable to *CDH1-2,3P* cells and significantly lower than wild type Clb2 levels.

A possible explanation of this result is that deletion of *CLN1* and *2* might allow for depolarizing bud growth and cell cycle progression in *CDH1-2,3P* cells with lower mitotic cyclin-CDK activity, by removing some yet unknown, Clb2-CDK independent, pathway that inhibits bud growth depolarization; although numerous other interpretations are possible. First, defects in *CDH1-2,3P* might be due to improper timing, not overall levels, of Clb2 accumulation, and deletion of *CLN1* and *2* might advance Clb2 accumulation without elevating overall levels. To test this, time-lapse experiments using a GFP-tagged Clb2 expressed from the native promoter would be required.

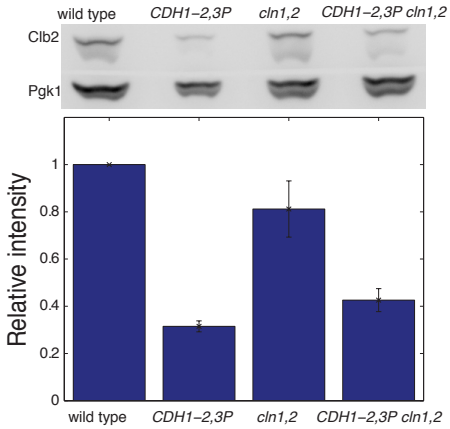

Figure 4.5: Western blotting for Clb2 levels in *CDH1-2,3P cln1,2* cells. Quantification was done by normalizing to Pgk1 intensity. Error bars represent standard error of the mean from three biological replicates.

Another possibility is that deletion of *CLN1* and *2* might restore levels of other mitotic cyclins Clb1,3 and 4, which are able to drive mitosis in absence of Clb2 (Richardson et al, 1992); western blotting for other mitotic Clbs would be required to evaluate this possibility. Another possibility is that Clb2 levels do not directly reflect Clb2-CDK kinase activity, since Clb2-CDK activity is also controlled both by posttranslational modifications (Sia et al, 1996), as well as the inhibitor Sic1 (Schwob et al, 1994). This could be addressed by kinase activity assays of immunoprecipitated Clb2-CDK complexes.

4.6. Conclusions and further directions

Taken together, the data reveal redundancy in APC-Cdh1 inactivation and suggest hierarchy among the negative regulators of APC-Cdh1. In addition to phosphorylation sites on Cdh1, where redundancy exists in the number of phosphorylation sites (chapter 3), I show here that multiple negative regulators of Cdh1 contribute to APC-Cdh1 inactivation in a redundant manner.

Phosphorylation of Cdh1 by CDKs is essential and therefore certainly the most important mode of regulation. However, phosphorylation of Cdh1 can be carried out by multiple cyclin-CDKs. Here, I present two pieces of evidence that Clb5-CDK, and its related partner Clb6-CDK, might be the main kinases responsible

for phosphorylation of Cdh1. Firstly, *CLB5* and *6* are required for timely inactivation of APC-Cdh1; in absence of *CLB5,6*, inactivation of APC-Cdh1 is delayed. However, clearly other, presumably later Clb-CDKs, are also capable of carrying out sufficient Cdh1 phosphorylation for cell cycle progression. Secondly, deletion of *CLB5* is lethal in combination with partially phosphorylatable CDH1 alleles lacking either the N-terminal (J. Robbins, PhD thesis) or the C-terminal subset of sites. This argues that phosphorylation of both of these subsets of sites might be carried out predominantly by Clb5-CDK, although, as noted above, other interpretations involving requirement for phosphorylation of other targets by Clb5-CDK, most plausibly Acm1, are possible.

In contrast, we found no indication for inhibitory phosphorylation of Cdh1 by Cln1 and 2-CDK. Direct measurement of timing of APC-Cdh1 inactivation in cells deleted for *CLN1* and *2* was impossible because of pleiotropic effects of Cln1 and 2; deletion of *CLN1* and *2* also affect the timing of budding, sharpness of Whi5 nuclear exit, as well as timing of expression of other Cdh1 regulators in the G1/S regulon. However, in contrast to *CLB5* and *6*, deletion of *CLN1* and *2* did not genetically interact negatively with partially phosphorylatable *CDH1* mutants, but paradoxically completely rescued the phenotypes associated with lack of Cdh1 phosphorylation sites. These results do not, however, conclusively prove that Cln1 and 2-CDK do not have a role in Cdh1 phosphorylation.

I currently do not have a plausible explanation for this unexpected result. A possible explanation would be that Cln1,2-CDK phosphorylates Cdh1 at specific sites in an activatory manner, and loss of this activatory phosphorylation by deletion of *CLN1* and *2* balances out the loss of inhibitory phosphorylation by other kinases; however, since the same genetic interaction was observed with two partially phosphorylatable alleles with non-overlapping subsets of sites, this explanation can be ruled out. Further experiments can be done by time-lapse microscopy using the APC-Cdh1 biosensor; this might reveal whether APC-Cdh1 is inactivated more completely in *CDH1-2,3P cln1,2* cells compared to *CDH1-2,3P* cells, although the interpretation of the results might be challenging due to APC-Cdh1-independent effects on biosensor degradation. Above, I also propose a few additional experiments to clarify whether deletion of *CLN1* and *2* in rescues the phenotype of *CDH1-2,3P* by restoring mitotic cyclin-CDK activity.

ACM1 is lower on the hierarchy of negative regulators of APC-Cdh1. Deletion of *ACM1* in wild type cells has no obvious growth or morphological defects, although a previous study has suggested that there might be occasional defects in nuclear positioning and spindle morphology in *acm1* cells (Martinez et al, 2012). Careful time-lapse microscopy experiments using the APC-Cdh1 biosensor might be able to reveal any defects in APC-Cdh1 inactivation in *acm1* cells.

However, deletion of *ACM1* was found to be deleterious when Cdh1 phosphorylation is impaired, either by removing a subset of phosphorylation sites, or deleting the likely main physiological kinases for Cdh1, *CLB5* and *6*. This suggests that inhibition by Acm1 likely serves as a buffer for occasional cell cycles when proper phosphorylation of Cdh1 fails.

I found no genetic interactions between *CDH1-2,3P* and deletion of *MSN5*. Previous experiments also showed no genetic interactions of *msn5* deletion with partially phosphorylatable *CDH1* alleles bearing other subsets of phosphorylation sites (J. Robbins, PhD thesis). Together, this suggests that Msn5 can promote nuclear export through interacting with multiple different phosphorylation sites on Cdh1, or that nuclear export of Cdh1 contributes so little to overall APC-Cdh1 inactivation that eliminating the nuclear export does not have any effects on cell viability. To assess the localization of Cdh1 protein throughout the cell cycle in partially phosphorylatable *CDH1* mutants, I attempted to construct a GFP-tagged version of *CDH1*; however, presumably due to low endogenous expression levels of *CDH1*, even when tagged with three repeats of fluorescent protein, the GFP signal was undetectable (data not shown). Overall, I therefore cannot evaluate the significance of nuclear export to APC-Cdh1 inactivation.

Chapter 5: Global analysis of cell cycle-regulated gene expression

The cell cycle progression in budding yeast is tightly linked to changes in gene expression, as approximately 20% of the yeast genome exhibits once per cell cycle oscillations of mRNA abundance. The main challenge at the present point is to understand to what extent this periodic gene expression is regulated by cyclin-CDK activity and therefore downstream of the CDK oscillator, and to what extent periodic gene expression is controlled by a "transcriptional oscillator", which was proposed to operate independently of the CDK oscillator (Orlando et al, 2008; Simmons-Kovacs et al, 2012).

In order to address this question, gene expression was measured in a strain where all cyclins were deleted and replaced with exogenously controlled G1 and mitotic cyclin. In this strain, tight control of cyclin expression allowed for complete depletion of all cyclin-CDK activity. A genome-wide gene expression time course experiment was performed and analyzed by principal component analysis. The experimental part of this work was done in collaboration with S. Jamal Rahi and Kresti Pecani.

5.1. Construction of strains and the time course experiment

For this experiment, two yeast strains were used. The experimental strain, named cln-clb-, had all three G1 cyclins *CLN1,2,3* deleted and replaced with a copy of *CLN2* driven by methionine-repressible promoter *MET3*. In addition, all the B-type cyclins *CLB1-6* were also deleted, and replaced by galactose-inducible *CLB2* (*GALL-CLB2*). The control strain, named cln-CLB+, also had the G1 cyclins deleted and replaced by *MET3-CLN2*, but retained all the *CLB* cyclins. The cln-clb- strain was viable on G-Met media where both *CLN2* and *CLB2* were constantly expressed, indicating that periodic gene expression of cyclins is not essential for cell cycle progression, even though the levels of Clb2 protein and Clb2-CDK kinase activity was substantially higher than in cyclin wild type cells in the same media condition (Rahi et al, submitted).

The previous experiment where gene expression in absence of B-type cyclins was measured (Orlando et al, 2008) was done in a strain where *GAL1-CLB1* was replacing all the B-type cyclins, but the activity of residual Clb1 upon shutoff was not measured, and it is possible that due to high expression level of *GAL1* promoter, residual *CLB1* could be present and could affect gene expression. For our cln-clb- strain, a protocol was devised in which the cells can be arrested in G1 completely depleted of any Clb2-CDK activity (1-2% of the wild type peak of total Clb-CDK activity; Rahi et al, submitted).

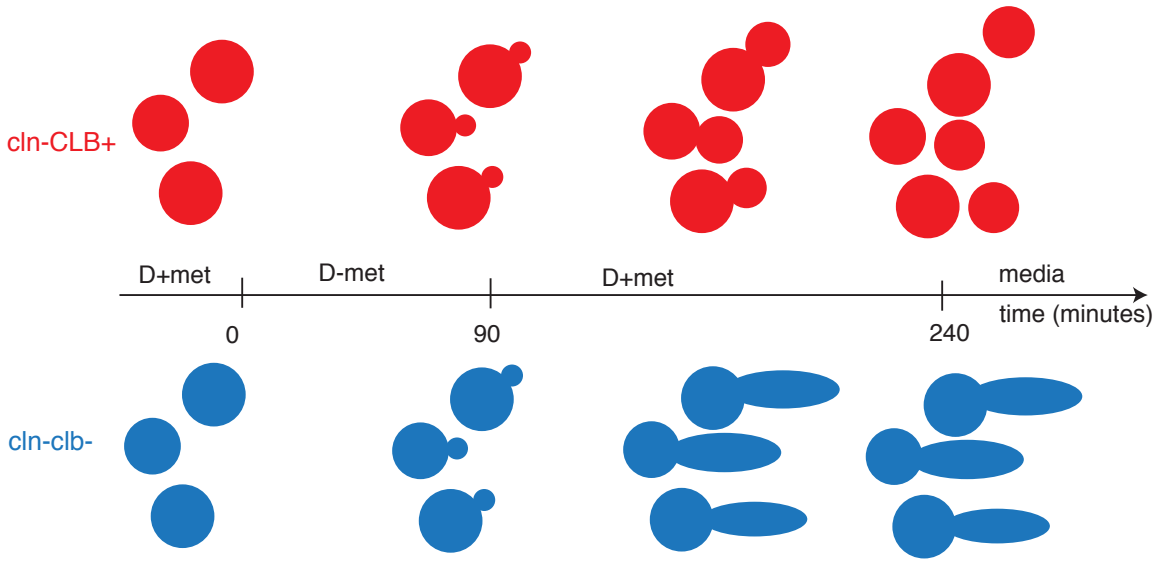

Figure 5.1: The scheme of the time course experiment for gene expression dynamics. Both cln-CLB+ (control) and cln-clb- cells were synchronized as unbudded cells in G1 by depleting G1 cyclins. -Met pulse for 90 minutes allowed expression of Cln2 and budding in both cells. cln-CLB+ cells proceeded to complete the cell cycle and arrested in subsequent G1 phase. cln-clb- cells were arrested at the G1/S border due to absence of B-type cyclins. Samples for transcriptome analysis were taken every 30 minutes. D, glucose; met, methionine.

The graphic scheme of the time course experiment is depicted in figure 5.1. Upon G1 arrest in Glu + met media where Clb2 was completely depleted (t=0 in the experiment), both strains were transiently shifted to media without methionine to transiently express *MET3-CLN2* for 90 minutes, after which methionine was added back to turn *MET3-CLN2* off. The transient expression of *CLN2* allowed for bud emergence in both strains. The control strains cells continued the cell cycle unperturbed until the next G1 phase, when they again arrested due to absence of G1 cyclins. Cln-clb- cells arrested after the transient -Met pulse as budded cells at the G1/S border, as their cell cycle progression was blocked due to absence of Clb-CDK activity. Aliquots of cultures were collected every 30 minutes and mRNA was isolated for transcriptome sequencing.

5.2. Dynamic transcriptional activity of cell cycle-regulated transcripts

Visual inspection of selected genes, previously associated with cell cycle regulation, revealed the dynamics of cell cycle regulons. The genes in the G1/S regulon, regulated by transcription factors SBF and MBF, peaked at 60 minutes, and the transcript abundance promptly decreased after (Figure 5.2 A). Both *TOS6* (a SBF target), as well as *RAD53* (an MBF target) also peaked in the cln-clb- cells.

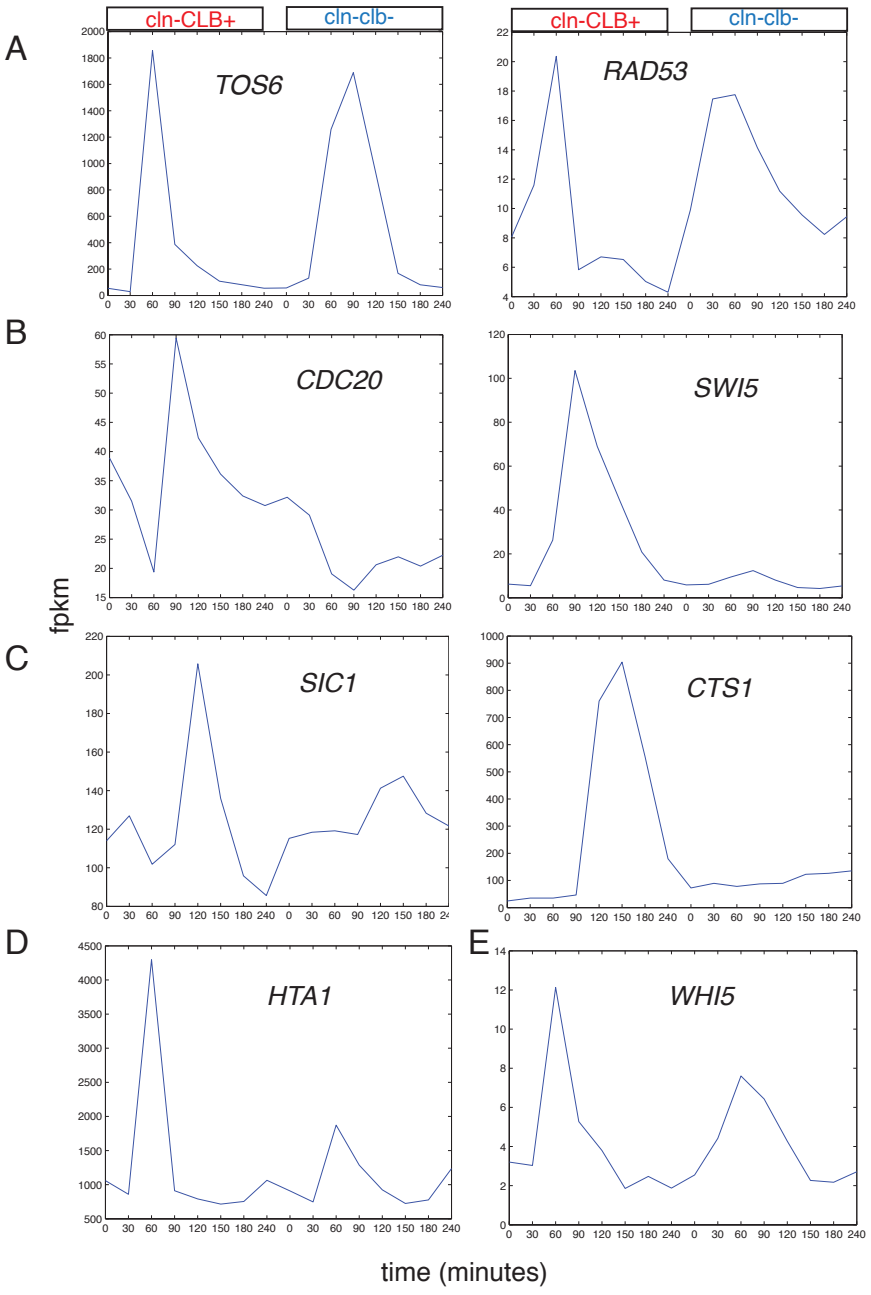

Figure 5.2: Transcript abundance of representative cell cycle-regulated genes. A; G1/S regulon. B; G2/M regulon (*CLB2* cluster). C; M/G1 regulon (*SIC1* cluster). D; histone cluster. E; S-phase cluster.

The genes from the second main regulon, the *CLB2* cluster (Spellman et al, 1998), regulated by the complex of Mcm1, Fkh1/2 and Ndd1 (Koranda et al, 2000; Reynolds et al, 2003), showed peak transcript abundance at 90 minutes (figure 5.2 B) in control cln-CLB+ cells. In contrast, no transcript of *SWI5* or *CDC20* genes in cln-clb- cells was detected. I note that this is in contrast with results by Orlando et al (2008), who observed reduced, but not absent activation of these genes (Orlando et al, 2008). Since requirement of mitotic cyclin activity for expression of *CLB2* cluster genes is well established (Amon et al, 1993), residual Clb1-CDK activity in the Orlando et al experiment might explain this discrepancy.

The genes from the late mitotic gene cluster (*SIC1* cluster, Spellman et al, 1998) peaked at t=120 min and t=150 min time points (figure 5.2 C). Interestingly, in cln-clb- cells, *SIC1* (a Swi5 target) expression was observed even though the amplitude was decreased compared to the control, but no *CTS1* (an Ace2 target) expression was observed.

I also examined genes belonging to additional regulatory clusters, the “histone cluster” (Spellman et al, 1998) and the S-phase cluster, regulated by Hcm1 (Pramila et al, 2006). Genes belonging to both of these clusters were activated at 60 minutes in control cells (Figure 5.2 D,E), making them indistinguishable in timing from the G1/S genes in this experiment due to limited time resolution.

Both *HTA1* (from the histone cluster) and *WHI5* (from the S-phase cluster) were also activated in cln-clb- cells with reduced amplitude.

5.3. Principal component analysis of the gene expression dataset

In order to gain insight into the global patterns of gene expression and global differences between the cln-CLB+ and cln-clb- cells, I performed principal component analysis (PCA) on the dataset in the matrix **A**. **A** is a 6717x16 matrix, each row representing one gene, and each column one time point sample (8 time point samples for each control and cln-clb- strain were collected). Preprocessing of the dataset to generate **A** is described in chapter 7 (Materials and methods).

PCA (also sometimes called singular value decomposition (SVD)) is a statistical method that produces a set of mutually orthogonal principal components. PCA is a commonly used procedure to reduce the dimensionality of the data by focusing on the main principal components that explain most of the variance. The transformation of the gene expression dataset matrix **A** according to the equation $\mathbf{A}=\mathbf{USV}^{\mathbf{T}}$ yields a set of 16 principal components, which are sets of uncorrelated, mutually orthogonal vectors, contained in matrices **U** and **V**.

The set of vectors in **U** represents “eigengenes”, an orthonormal set of vectors that explain variance among the genes (mathematically, eigengenes are eigenvectors of the covariance matrix $\mathbf{A}^T\mathbf{A}$). The set of vectors in **V** represents “eigensamples”, an orthonormal set of vectors that explains the variance among the time point samples (mathematically, eigenvectors of the covariance matrix $\mathbf{A}\mathbf{A}^T$).

The first four principal components explain 50% of the total variance (table 1) of the dataset. The first two principal components each explain about 15% of the variance. The mathematics of the PCA suggests focusing on the principal components that explain a higher fraction of variance.

Here, I plot the time profiles of the first four eigengenes. The profile of the first eigengene shows a different pattern between the control and cln-clb- strains (figure 5.3). For the control strain, it showed a broad peak at timepoints from 90 to 180 minutes. For the cln-clb- strain, it remained constant at low levels for the entire experiment. In contrast, the second eigengene showed a very pattern for both strains, with both the control and cln-clb- strains exhibiting a sharp peak at the 60 minutes timepoint.

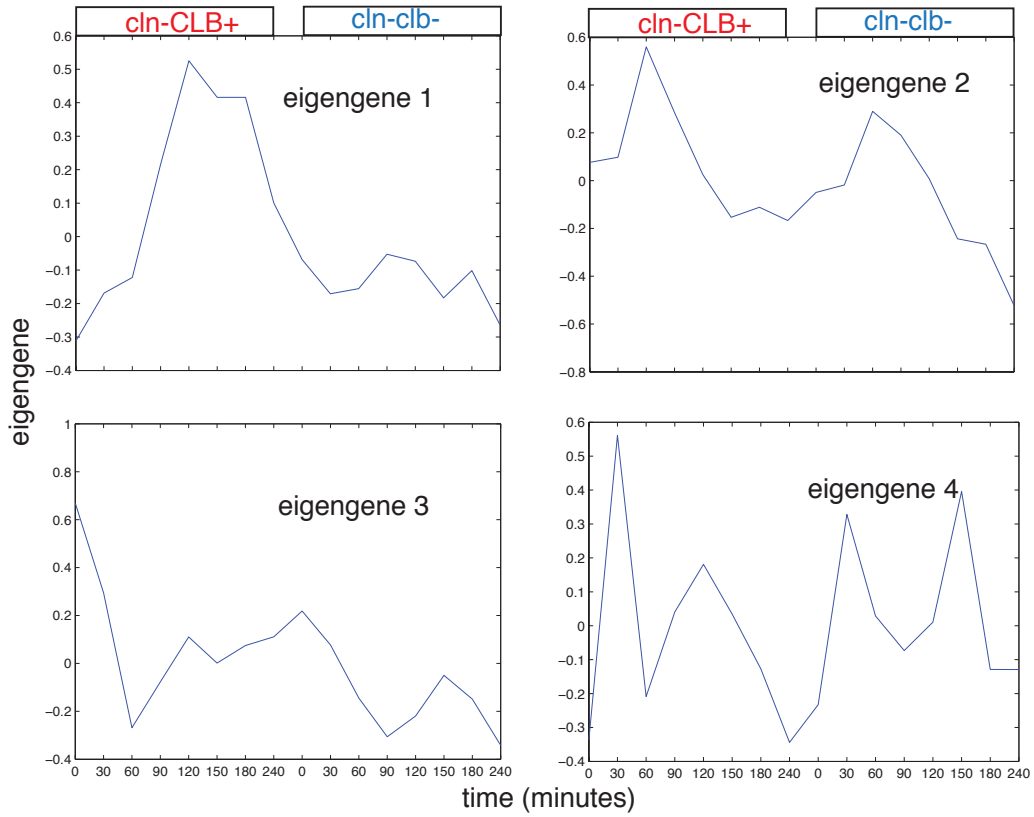

Figure 5.3: Time profiles of eigengenes associated with the four highest singular values.

Principal component	Fraction of variance explained
1	0.15
2	0.15
3	0.11
4	0.08
Sum (5-16)	0.51

Table 5.1: Fraction of variance explained by individual principal components.

The third and fourth eigengenes, which explain 11 and 8 % of variance in the dataset, respectively, also showed different dynamics for the control and cln-clb- strain, with peaks and troughs at different timepoints. Further analysis was focused on first two principal components.

5.4. Clustering of co-regulated genes in the eigengene space

Gene profiles for each individual gene were projected onto the subspace spanned by the first two principal components, and combined that with functional classification of genes based on published information on their transcriptional regulation (Figure 5.4).

On the scatter plot, genes from the dataset of annotated SBF and MBF targets (Ferrezuelo et al, 2010) are plotted in green. On the PC1/PC2 subspace, genes from this regulon are largely clustered along the PC2 axis, implying high correlation of their profiles with the eigengene 2 (figure 5.4).

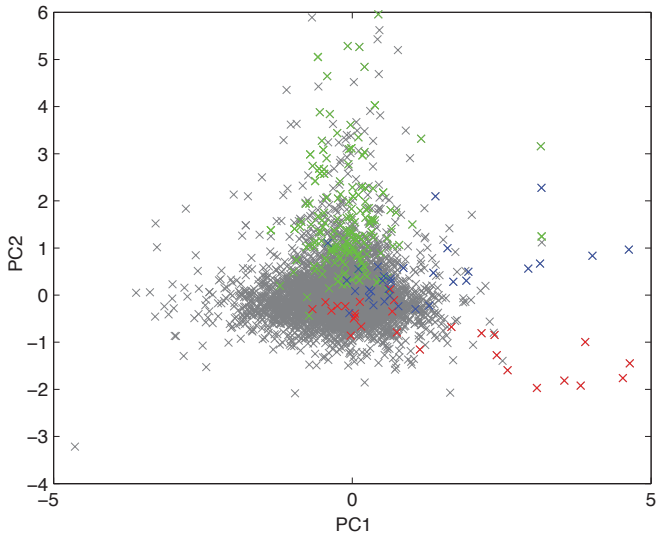

Figure 5.4: Projections of genes onto the subspace of the first two eigengenes. Each dot represents one of the genes (total 6717). Green, genes identified as SBF and MBF targets. Blue, genes from the *CLB2* cluster. Red, genes from the *SIC1* cluster.

Genes identified as members of the "*CLB2* cluster" and "*SIC1* cluster" (Spellman et al, 1998) were plotted in blue and red, respectively. Both of these gene clusters localized in the region of high correlation with PC1 (figure 5.4). However, the two clusters were separated from each other. The CLB2 cluster genes were observed in the upper right area in the region with slightly positive contribution of the PC2. The SIC1 cluster genes were located below in the region with slightly negative contribution of PC2.

This results suggests that projecting genes onto the subspace spanned by the first two principal components generates clusters of co-regulated genes, which provides validation of the analysis based on the first two principal components. Further work could be done to analyze other groups of genes based on known transcriptional co-regulation, as well as groups of genes based on other functional categories.

5.5. Projection onto eigensample space reveals global gene expression trajectories

Plotting of projections of successive time point samples onto the subspace of eigensamples 1 and 2 revealed differences between the cln-CLB+ control and cln-clb- datasets (figure 5.5). Overall, the trajectories of the two time courses are

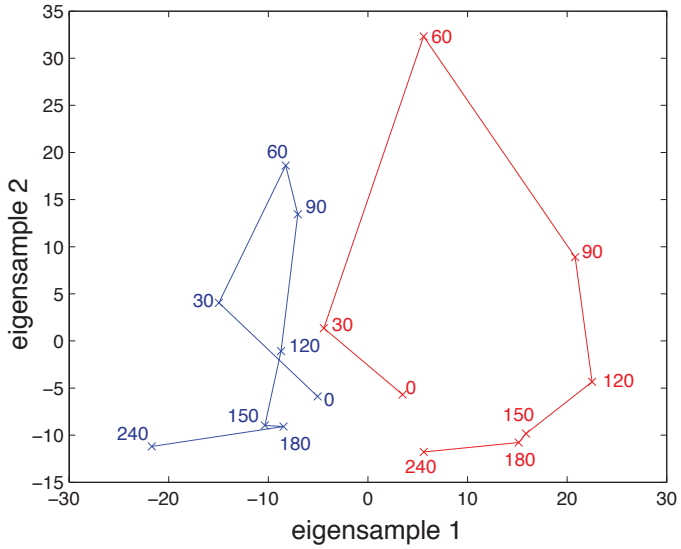

Figure 5.5: Projections of samples onto the subspace of the first two eigensamples. Numbers on the plot indicate time points in minutes. Red; cln-CLB+ samples. Blue; cln-clb- samples.

strongly separated along the PC1 axis. The time course of the control strain (figure 5.5, red line) started close to the origin. Subsequently, the contribution of the second principal component increased strongly at t=60min time point, followed by an increase of the contribution of the PC1 while the contribution of the PC2 decreased, and ultimately returned to the starting point to form a closed orbit. This is consistent with a near-complete return of the cells to the starting condition of the experiment.

The time course of the cln-clb- dataset (figure 5.5, blue line) initially paralleled the control time course trajectory. However, the increase of the contribution of PC2 at the 60 minute timepoint was smaller. After the 60 min timepoint, the cln-clb- dataset diverged drastically from the control dataset, immediately returning close to the starting condition at t=90 min and remained there.

This result has a biological interpretation and implies differential patterns of global gene expression between the control and cln-clb- cells. The global gene expression between the cln-CLB+ and cln-clb- strains changed dramatically starting at the t=90 minutes, corresponding to the timing of the expression of the CLB2 cluster regulon. Therefore, expression of later cell cycle-transcriptome after the 60 minute time point is significantly affected in the cln-clb- strain.

5.6. Conclusions and further directions

Here, I describe a preliminary attempt to analyze the genome-wide gene expression pattern using principal component analysis. The main motivation was to compare gene expression pattern of the strain that was lacked all the B-type cyclins with a control strain. PCA was used before to analyze the budding yeast cell cycle gene expression data (Alter et al, 2000), and more recently also to analyze diurnal gene expression in green alga *Chlamydomonas reinhardtii* (Tulin and Cross, submitted). Unlike other methods used before to analyze gene expression patterns, such as k-means clustering (Eisen et al, 1998) or identifying cell cycle-regulated gene expression patterns by comparing with idealized gene profiles (de Lichtenberg et al, 2005; Orlando et al, 2008), PCA does not require input of any arbitrary parameters and is model-independent.

Generally, individual eigengenes are only expected to directly reflect some underlying biological pattern in case the biological patterns are mutually orthogonal. This, in general, depends strongly on the nature of the data, and can also be affected by preprocessing of the data.

I analyzed the data in terms of the first two principal components, which together explain 30% of the variance of the dataset. I find that the G1/S regulon genes correlate strongly with the second principal component, whereas the later

expressed gene regulons (CLB2 cluster and SIC1 cluster) correlate with the first principal component. In the subspace spanned by the first two principal components, the three main cell cycle gene regulons occupy distinct clusters.

Furthermore, the analysis provides a clear insight into the effects of B-type cyclins on the gene expression patterns. Contrary to previous analysis, which highlighted the lack of change in gene expression patterns in cells without B-type cyclins (Orlando et al, 2008), principal component analysis of the present dataset revealed effects of B-type cyclin deletion. Analyzed in terms of the subspace of the first two principal components, the gene expression patterns of the control and cln-clb- strain diverged greatly after 60 minutes, indicating that the gene expression of later genes, but not the G1/S regulon, is affected in the B-type cyclin mutant cells.

Presently, the focus was on the first two principal components, which was sufficient to explain the main patterns in the dataset, and the additional principal components were ignored. Principal components that explain smaller degree of variance are generally assumed to only reflect noise in the dataset; however, analyzing the data in terms of additional principal components might reveal additional details about the experiment. In addition, further insights might be gained by improving the temporal resolution of the experiment; while 30 minute sampling interval is sufficient for temporal differentiation of the three major

regulons, finer sampling might reveal subtler temporal differences in expression between genes in the same regulon, and changes in timing between control and cln-clb- cells.

Chapter 6: Discussion

Timing of APC-Cdh1 inactivation

In this work, I measured the timing of APC-Cdh1 inactivation at the single cell resolution.

The events associated with the Start transition in budding yeast were previously shown to be relatively coherent, with some coherence between the events likely sacrificed to ensure timely completion of all events (Bean et al, 2006). Inactivation of APC-Cdh1, as shown here, is highly coherent with Whi5 exit, but poorly coherent with bud emergence. This is, as shown before, due to substantial variability of timing of bud emergence with respect to Whi5 exit (Di Talia et al, 2007).

Whi5 exit is the regulatory step that ensures expression of multiple genes that contribute to APC-Cdh1 inactivation; which subcomponents of the Start regulatory network contribute to timely APC-Cdh1 inactivation remains to be addressed.

I speculate that the difference in observed timing variability between APC-Cdh1 inactivation and bud emergence might be rationalized by differential selection

pressure for reducing variability. The timing variability in bud emergence might be tolerated because budding is regulatorily decoupled from downstream cell cycle events, and bud growth is likely not rate limiting for cell cycle progression. In contrast, inactivation of APC-Cdh1 is an essential step for immediate downstream events, such as accumulation of mitotic cyclins, and, as also shown in this work, activation of expression of the mitotic cyclins. Therefore, a delay in APC-Cdh1 inactivation could be rate-limiting for subsequent cell cycle events. The architecture of the Start molecular network has likely been designed to prioritize noise suppression in inactivation of APC-Cdh1 over bud emergence.

Requirement for multisite phosphorylation of Cdh1 for APC-Cdh1 inactivation

The experiments presented here contribute to our understanding of how the multisite phosphorylation of Cdh1 works. Previously, it has been shown that no single site is essential, and that contribution of phosphorylation sites is unequal, implying regulation by bulk charge with some regional specificity (J. Robbins, PhD thesis). Here, I further show that no single phosphorylation site is sufficient for proper inhibition of APC-Cdh1 activity.

Multiple partially phosphorylatable *CDH1* mutants showed stochastic cell cycle defects in individual cells. Further characterization of the phenotype of one of these mutants revealed a partially penetrant phenotype in cell cycle progression. A fraction of the cells completed the cell cycle, and even the cells that resembled the fully arrested cells continued to perform some cell cycle events. This phenotype was, as measured using the assay for APC-Cdh1 activity, associated by incomplete but partial restrainment of APC-Cdh1 activity. However, due to the complex phenotype, precise quantification of the requirement for APC-Cdh1 inactivation remains unknown.

Mechanism of APC-Cdh1 inactivation by phosphorylation at the N-terminal sites

A high-resolution of structure of the APC bound to Cdh1 has revealed the interface between Cdh1 and APC (Schreiber et al, 2011). Notably, the N-terminal sites, which were shown to have the strongest contribution to APC-Cdh1 inactivation, are located in the unstructured region of Cdh1 that maps into the unassigned density in the structure that likely links Cdh1 and the C-terminus of Apc2 (Schreiber et al, 2011; D. Barford, personal communication), implying a direct physical interaction of the N-terminus of Cdh1 with Apc2. This structural detail might provide an insight into the biochemical mechanism of inhibition by

phosphorylation at the N-terminal sites, and further biochemical experiments could be designed to test this directly.

Cyclin specificity in Cdh1 phosphorylation

Here, I add two additional pieces of evidence that suggest that Cdh1 might be predominantly phosphorylated by Clb5-CDK (and possibly its less potent partner Clb6-CDK) in vivo. Multiple lines of evidence for the role of Clb5-CDK already exist. Substrate specificity of Clb5-CDK is determined by presence of the RXL motif on the substrate; such a motif exists in Cdh1, and Cdh1 was preferentially phosphorylated by Clb5-CDK compared to Clb2-CDK in cell lysates (Loog and Morgan, 2005).

Here, I show that in absence of Clb5 and 6, inactivation of APC-Cdh1 is delayed. This result was shown by measurement in single cells and the delay was quantified; however a qualitative observation of the delay in APC-Cdh1 in absence of Clb5 and 6 has been shown before (Huang et al, 2001). This indicates that Clb5 and/or 6-CDK are likely the physiological kinase for Cdh1 in wild type cells, although in their absence, other kinases can carry out physiologically sufficient Cdh1 phosphorylation with a delay or with reduced efficiency.

Second, deletion of *CLB5* was shown to be lethal in combination of mutation of either the C-terminal or N-terminal sites. The likely interpretation of this result is that when phosphorylation of Cdh1 becomes impaired, other kinases become insufficient for efficient or timely phosphorylation at the remaining sites, implying a strong contribution of Clb5-CDK to phosphorylation of both of these subsets of sites. However, this genetic interaction can also be interpreted by indirect effects of *clb5* deletion.

In contrast, assessing the role of Cln1 and 2-CDK in APC-Cdh1 inactivation revealed an opposite result, as deletion of *CLN1,2* in partially phosphorylatable CDH1 context paradoxically alleviated the phenotype associated with incomplete APC-Cdh1 inactivation. This result is at present difficult to reconcile with the current understanding of the budding yeast cell cycle control. This genetic interaction does not exclude the possibility that any phosphorylation of Cdh1 by Cln1,2-CDK occurs; however, it points at that another additional mechanism of APC-Cdh1 regulation by Cln1,2-CDK that is presently not understood. Further characterization is required to understand the mechanism of the rescue and explain the complete role of Cln1,2-CDK in APC-Cdh1 regulation.

The global cell cycle transcriptional program requires B-type cyclins

I addressed the global cell cycle regulatory program. The current unresolved controversy is to what extent cell cycle-regulated transcription is, like the majority of other cell cycle events, regulated by oscillations of cyclin-CDK activity, and to what extent the periodic transcriptional program is autonomously driven by a proposed transcription factor oscillator (Orlando et al, 2008; Simmons-Kovacs et al, 2012).

To address the question, I performed principle component analysis on the global gene expression dataset generated from the time course of cells lacking all B-type cyclins, along with control cells. The results of the principal component analysis showed that the global transcriptional pattern is largely absent in B-type cyclin mutant cells. This result implies the requirement for B-type cyclin-CDK activity for the global periodic transcriptional program.

However, it must be noted that the absence of a global pattern of periodic gene activation does not preclude that some individual genes might still be activated in absence of Clb-CDK activity. In fact, a small subset of M/G1 genes, most notably including *SIC1*, a gene coding for an inhibitor of B-type cyclin kinases, was found to be expressed in absence of Clb-CDK activity. Given the function of

Sic1 in the budding yeast cell cycle, a mechanism for Clb-CDK-independent transcriptional induction has been proposed (Rahi et al, submitted).

Chapter 7: Materials and methods

Strains and plasmid construction

Standard methods for strain constructions were used throughout. All strains are W303-congenic. Strains and plasmids used in this work are listed in tables 7.1 and 7.2, respectively. The APC-Cdh1 biosensor plasmid was constructed by amplifying the *ASE1* degron sequence from the plasmid PB1452 (obtained from David Pellman) and cloned into the pGC25 plasmid to obtain pAO4, which was linearized with XbaI to integrate into the *TRP1* locus. The following oligonucleotides were used for cloning:

Ase1degr-f-COR:

GGTATTACCCATGGTATTGATGAATTGTACAAAAGATCTAAAAAGGGAAAATGTGGTGCG

Ase1degr-r:

TCGCTTATTTAGAAGTGGCGCGCCTTATCAAATATCTGTAAAGGAGAATCCATTC

The pAO1, pAO2 and pAO3, pAO16-23P and pAO16-13P plasmids bearing CDH1 phosphomutants were generated by subcloning AvaI/BlpI fragments (containing the N-terminal parts of the *CDH1* ORF) from JRP64, JRP63, JRP62, JRP60 and JRP78, respectively, into FC687. The plasmid was then linearized with BglII to integrate into the *CDH1* locus. The transformants were then

subjected to 5-FOA selection. This generated colonies of both wild-type *CDH1* and desired phosphomutant depending on the site of homologous recombination; colonies were screened by sequencing the PCR product.

Media and culture conditions

Standard media and liquid culture conditions were used. Fluorescence imaging experiments were performed with cultures grown in synthetic media to minimize autofluorescence.

Fluorescence time-lapse microscopy and image analysis

Time lapse imaging and subsequent automated image segmentation was performed using the instrumentation and software as described previously (Charvin et al, 2008), with a difference that cells grown in a commercial microfluidic chamber (CELLAsic, Hayward, CA) as per manufacturer instructions. Images were acquired every 3 minutes. Subsequent data analysis was performed in Matlab. Image segmentation was done semi-automatically. Fluorescence trace smoothing was performed using the Matlab function “smooth” with the method “lowess” over the 10 time points. Nuclear fluorescence

was measured by either manually detecting nuclei from the images, or computed from the images as described (Charvin et al, 2010). In experiments using both GFP and YFP, fluorescence in both channels was recomputed to correct for spectral bleed-through using empirically determined parameters.

DIC microscopy

DIC images were taken using an Axioplan 2 microscope (Carl Zeiss, Thornwood, NY) and a 63x NA 1.4 Plan APO objective. The camera and the microscope were controlled by the OpenLab software.

Immunoblotting

Immunoblots were performed using standard protocols. The antibodies (rabbit polyclonal anti-Clb2 and anti-Pgk1 (Invitrogen, Carlsbad, CA)), were used in 1:10000 concentrations. Enhanced chemiluminescence signal was measured with DarkBox (Fujifilm, Greenwood, SC) with a charge-coupled device camera and quantified using MultiGauge software (Fujifilm). Quantification was performed using ImageJ.

Transcriptome analysis

Total RNA was isolated from collected samples using the Trizol reagent. cDNA libraries were prepared using Illumina TruSeq sample preparation kit. Sequencing was performed by Genewiz (South Plainfield, NJ) and was done on the Illumina HiSeq2500 platform in a 1x50bp single-read configuration in Rapid Run mode.

Data preprocessing

The mRNA sequencing data were expressed as fpkm (fragments per kilobase per million reads). The reads for each strain and time point were normalized to the same total reads. The time course was performed in biological duplicates; the datasets were normalized to each other before averaging. The matrix contained 6717 rows, each corresponding to one gene, and 16 columns, corresponding to time point samples (8 for the cln-CLB+ control, 8 for the cln-clb-). Before performing PCA, each row was normalized by mean expression and subtracted 1 to center each gene profile at 0. Finally, genes with mean expression below 3 fpkm were filtered out; these low fragment counts are almost surely not biologically relevant, and noise from these random fluctuations was

found to significantly dominate the principal component analysis if not filtered out. This generated the data matrix **A**.

Principal component analysis

Principal component analysis was performed in Matlab using the command svd, which generated 3 matrices according to the equation $\mathbf{A}=\mathbf{USV}^{\mathbf{T}}$, where **A** is the matrix containing the gene expression data. The matrix **S** is a diagonal matrix containing singular values (weights of each principal component). The matrix **U** contains column vectors, “eigensamples”, that are eigenvectors of the covariance matrix $\mathbf{AA}^{\mathbf{T}}$. Finally, the matrix **V** contains column vectors, “eigengenes”, that are eigenvectors of $\mathbf{A}^{\mathbf{T}}\mathbf{A}$.

Projections of genes onto the subspace of the first two principal components were calculated as dot products of rows of the matrix **A** with the first two eigengenes (for the figure 5.4). The projections of samples were calculated as dot products of each column of the matrix **A** with the two eigensamples.

Table 7.1: List of strains used in this work.

GC46-03	*MATa MYO1-mCherry-HIS5*
AO832-3c	*MATalpha MET3pr-yVENUS-ASE1deg-TRP1::trp1 MYO1-mCherry-HIS5*
AO852-2d	*MATalpha MET3pr-yVENUS-ASE1deg-TRP1::trp1 MYO1-mCherry-HIS5 cdh1::LEU2*
AO602-11d	*MATa MET3pr-yVENUS-ASE1deg-TRP1::trp1 GALL-CDC20-ADE2::ade2 cdc20::LEU2*
AO95-4a	*MATalpha MET3pr-yVENUS-ASE1deg-TRP1::trp1 MYO1-mCherry-HIS5 GALL-ACM1-LEU2::leu2 CDH1-m11*
AO261-5b	*MATa MET3pr-yVENUS-ASE1deg-TRP1::trp1 WHI5-GFP-KanMX HTB2-mCherry-HIS5*
AO1221-12c	*MAT? MET3pr-yVENUS-ASE1deg-TRP1::trp1 MYO1-mCherry clb5::HIS3 clb6::KanMX*
AO7-1p1	*MATa GALL-ACM1-LEU2::leu2 CDH1-1P*
AO7-2p2	*MATa GALL-ACM1-LEU2::leu2 CDH1-2P*
AO7-3p3	*MATa GALL-ACM1-LEU2::leu2 CDH1-3P*
AO17-13P1	*MATa GALL-ACM1-LEU2::leu2 CDH1-1,3P*
AO17-23P	*MATa GALL-ACM1-LEU2::leu2 CDH1-2,3P*
3149-21	*MATa GALL-ACM1-LEU2::leu2 CDH1-m11*
AO761-8b	*MATa GALL-ACM1-LEU2::leu2 CDH1-2,3P MYO1-mCherry-HIS5 MET3-yVENUS-ASE1deg-TRP1::trp1*
AO812-12c	*MATa GALL-ACM1-LEU2::leu2 CDH1-2,3P MYO1-mCherry-HIS5 CLB2-GFP-HIS5*
AO87-4c	*MATa GALL-ACM1-LEU2::leu2 CDH1-m11 MYO1-mCherry-HIS5 CLB2-GFP-HIS5*
AO712-11c	*MATa GALL-ACM1-LEU2 MYO1-mCherry-HIS5 CLB2pr-GFP-KanMX CDH1-2,3P*
AO64-1c	*MATalpha GALL-ACM1-LEU2 MYO1-mCherry-HIS5 CLB2pr-GFP-KanMX CDH1-m11*
AO632-6c	*MATa GALL-ACM1-LEU2 MYO1-mCherry-HIS5 SIC1pr-YFP-URA3 CDH1-m11*
AO70-6d	*MATalpha GALL-ACM1-LEU2 MYO1-mCherry-HIS5 SIC1pr-YFP-URA3 CDH1-2,3P*
AO632-4b	*MATa GALL-ACM1-LEU2 MYO1-mCherry-HIS5 SIC1pr-YFP-URA3*
yLB5	*MATa MYO1-mCherry-HIS5 CLN2pr-GFP-URA3*
AO72-5c	*MATa GALL-ACM1-LEU2 MYO1-mCherry-HIS5 CLN2pr-GFP-URA3 CDH1-m11*
AO681-1c	*MATa GALL-ACM1-LEU2 MYO1-mCherry-HIS5 CLN2pr-GFP-URA3 CDH1-2,3P*
AO86-6b	*MATa MYO1-mCherry-HIS5 CLB2-GFP-HIS5*
JRC397A-1c	*MATa GAL1-ACM1-URA3::ura3 acm1::KanMX msn5::HIS3*

JRC397A-9b	*MATa GAL1-ACM1-URA3::ura3 acm1::KanMX*
JRC397A-9b	*MATa GAL1-ACM1-URA3::ura3 msn5::HIS3*
MNX33-1d	*MATa GAL1-ACM1-URA3::ura3 CDH1-5:11P acm1::KanMX msn5::HIS3*
MNX33-3c	*MATa GAL1-ACM1-URA3::ura3 CDH1-5:11P msn5::HIS3*
MNX33-7d	*MATa GAL1-ACM1-URA3::ura3 CDH1-5:11P acm1::KanMX*
AO88-10a	*MATa GALL-ACM1-LEU2::leu2 CDH1-2,3P acm1::KanMX msn5::HIS3*
AO88-7c	*MATa GALL-ACM1-LEU2::leu2 CDH1-2,3P acm1::KanMX*
AO88-10b	*MATalpha GALL-ACM1-LEU2::leu2 CDH1-2,3P msn5::HIS3*
AO89-7b	*MATa GALL-ACM1-LEU2::leu2 CDH1-2,3P clb6::KanMX clb5::HIS3*
AO89-10a	*MATa GALL-ACM1-LEU2::leu2 CDH1-2,3P clb6::KanMX*
AO89-11b	*MATalpha GALL-ACM1-LEU2::leu2 CDH1-2,3P clb5::HIS3*
JRC437A-6a	*MATa GAL1-ACM1-URA3::ura3 CDH1-5:11P clb6::KanMX clb5::HIS3*
JRC437A-4d	*MATa GAL1-ACM1-URA3::ura3 CDH1-5:11P clb5::HIS3*
JRC437A-9c	*MATa GAL1-ACM1-URA3::ura3 CDH1-5:11P clb6::KanMX*
JRC436A-6c	*MATa GAL1-ACM1-URA3::ura3 clb5::HIS3*
JRC436A-1c	*MATa GAL1-ACM1-URA3::ura3 clb6::KanMX*
JRC436A-1d	*MATa GAL1-ACM1-URA3::ura3 clb6::KanMX clb5::HIS3*
AO1272-7d	*MAT? GALL-ACM1-LEU2::leu2 clb6::KanMX clb5::HIS3 acm1::NatMX*
AO1272-2d	*MAT? GALL-ACM1-LEU2::leu2*
AO1271-5b	*MAT? GALL-ACM1-LEU2::leu2 clb6::KanMX clb5::HIS3*
AO1271-5a	*MAT? GALL-ACM1-LEU2::leu2 acm1::NatMX*
AO1192-9a	*MATa GALL-ACM1-LEU2::leu2 MET3-CLN2-TRP1::trp1 MYO1-mCherry-HIS5*
AO1194-6b	*MAT? GALL-ACM1-LEU2::leu2 MET3-CLN2-TRP1::trp1 cln1 cln2 MYO1-mCherry-HIS5*
AO939-7b	*MATa GALL-ACM1-LEU2::leu2 MET3-CLN2-TRP1::trp1 CDH1-2,3P*
AO939-7a	*MATa GALL-ACM1-LEU2::leu2 MET3-CLN2-TRP1::trp1 CDH1-2,3P cln1 cln2 MYO1-mCherry*
AO1017-3d	*MAT? GAL1-ACM1-URA3::ura3 MET3-CLN2-TRP1::trp1 CDH1-5:11P cln1 cln2*
AO1012-10b	*MAT? GAL1-ACM1-URA3::ura3 MET3-CLN2-TRP1::trp1 CDH1-5:11P*
AO123-4a	*MAT? GALL-ACM1-LEU2::leu2 GAL1-SIC1-TRP1::trp1 CDH1-2,3P CLB2-ken*
AO123-7a	*MAT? GALL-ACM1-LEU2::leu2 GAL1-SIC1-TRP1::trp1*

	CLB2-ken
AO123-5d	*MAT? GALL-ACM1-LEU2::leu2 GAL1-SIC1-TRP1::trp1 CDH1-2,3P*
AO1261-3b	*MAT? GALL-ACM1-LEU2::leu2 MET3-yVENUS-ASE1deg-TRP1::trp1 MYO1-mCherry-HIS5 CDH1-2,3P CLB2-ken*
AO-44-4	*MATa MYO1-mCherry-HIS5 CLB2::CLB2pr-GFP-LEU2*
AO-1271-5a	*MAT? GALL-ACM1-LEU2 acm1::NatMX*
AO-1271-5b	*MAT? GALL-ACM1-LEU2 clb5::HIS3 clb6::KanMX*
AO-1272-2d	*MAT? GALL-ACM1-LEU2*
AO-1272-7d	*MAT? GALL-ACM1-LEU2 clb5::HIS3 clb6::KanMX acm1::NatMX*
2773-1D	*MATa cln1 cln2 cln3::LEU2 MET3-CLN2-TRP1*
SJR27a7b	*MAT? cln1 cln2 cln3::LEU2 MET3-CLN2-TRP1 clb1 clb6::KanMX clb2::GAL-CLB2-URA3 clb5::KanMX clb3::TRP1 clb4::his3::KanMX SIC1::SIC1pr-YFP-URA3*

Table 7.2: List of plasmids used in this work.

pAO4	*pRS404 MET3pr-Ase1deg-VENUS*
PB1452	*GAL1-ASE1degron-GST*
pGC25	*pRS404 MET3pr-VENUS*
pAO1	*pRS406 CDH1-1P*
pAO2	*pRS406 CDH1-2P*
pAO3	*pRS406 CDH1-3P*
pAO16-23P	*pRS406 CDH1-2,3P*
pAO16-13P	*pRS406 CDH1-1,3P*
FC687	*pRS406 CDH1-m11*
JRP64	*pRS406 CDH1-S16A-T42A-T157A*
JRP60	*pRS406 CDH1-T12A-T157A*
JRP63	*pRS406 CDH1-T12A-T42-T157A*
JRP62	*pRS406 CDH1-T42-T157A*
JRP78	*pRS406 CDH1-S16A-T157A*

References

Alter, O., Brown, P.O. and Botstein, D. (2000) Singular value decomposition for genome-wide expression data processing and modeling. *Proc Natl Acad Sci U S A*, **97**, 10101-6.

Altschuler, S.J. and Wu, L.F. (2010) Cellular heterogeneity: do differences make a difference? *Cell*, **141**, 559-63.

Amon, A., Tyers, M., Futcher, B. and Nasmyth, K. (1993) Mechanisms that help the yeast cell cycle clock tick: G2 cyclins transcriptionally activate G2 cyclins and repress G1 cyclins. *Cell*, **74**, 993-1007.

Balaban, N.Q., Merrin, J., Chait, R., Kowalik, L. and Leibler, S. (2004) Bacterial persistence as a phenotypic switch. *Science*, **305**, 1622-5.

Bean, J.M., Siggia, E.D. and Cross, F.R. (2006) Coherence and timing of cell cycle start examined at single-cell resolution. *Mol Cell*, **21**, 3-14.

Benmaamar, R. and Pagano, M. (2005) Involvement of the SCF complex in the control of Cdh1 degradation in S-phase. *Cell Cycle*, **4**,1230-2.

Bristow, S.L., Leman, A.R., Simmons Kovacs, L.A., Deckard, A., Harer, J and Haase, S.B. (2014) Checkpoints couple transcription network oscillator dynamics to cell-cycle progression. *Genome Biol*, **15**, doi:10.1186.

Cagatay, T., Turcotte, M., Elowitz, M.B., Garcia-Ojalvo, J. and Suel, G.M. (2009) Architecture-dependent noise discriminates functionally analogous differentiation circuits. *Cell*, **139**, 512-22.

Charvin, G., Cross, F.R. and Siggia, E.D. (2008) A microfluidic device for temporally controlled gene expression and long-term fluorescent imaging in

unperturbed dividing yeast cells. *PLoS One*, **3**, e1468.

Charvin, G., Oikonomou, C., Siggia, E.D. and Cross, F.R. (2010) Origin of irreversibility of cell cycle start in budding yeast. *PLoS Biol*, **8**, e1000284.

Cohen-Fix, O., Peters, J.M., Kirschner, M.W. and Koshland, D. (1996) Anaphase initiation in Saccharomyces cerevisiae is controlled by the APC-dependent degradation of the anaphase inhibitor Pds1p. *Genes Dev*, **10**, 3081-3093.

Colman-Lerner, A., Chin, T.E. and Brent, R. (2001) Yeast Cbk1 and Mob2 activate daughter-specific genetic programs to induce asymmetric cell fates. *Cell*, **107**, 739-50.

Crasta, K., Lim, H.H., Giddings, T.H., Jr., Winey, M. and Surana, U. (2008) Inactivation of Cdh1 by synergistic action of Cdk1 and polo kinase is necessary for proper assembly of the mitotic spindle. *Nat Cell Biol*, **10**, 665-675.

Cross, F.R. and Tinkelenberg, A.H. (1991) A potential positive feedback loop controlling CLN1 and CLN2 gene expression at the start of the yeast cell cycle. *Cell*, **65**, 875-883.

Cross, F.R., Archambault, V., Miller, M. and Klovstad, M. (2002) Testing a mathematical model of the yeast cell cycle. *Mol Biol Cell*, **13**, 52-70.

de Lichtenberg, U., Jensen, L.J., Fausboll, A., Jensen, T.S., Bork, P. and Brunak, S. (2005) Comparison of computational methods for the identification of cell cycle-regulated genes. *Bioinformatics*, **21**, 1164-71

Deshaies, R.J. and Ferrell, J.E., Jr. (2001) Multisite phosphorylation and the countdown to S phase. *Cell*, **107**, 819-822.

Di Fiore, B. and Pines, J. (2007) Emi1 is needed to couple DNA replication with mitosis but does not regulate activation of the mitotic APC/C. *J Cell Biol*, **177**, 425-37.

Di Talia, S., Skotheim, J.M., Bean, J.M., Siggia, E.D. and Cross, F.R. (2007) The effects if molecular noise and size control on variability in the budding yeast cell cycle. *Nature*, **448**, 947-51.

Dirick, L. and Nasmyth, K. (1991) Positive feedback in the activation of G1 cyclins in yeast. *Nature*, **351**, 754-757.

Dirick, L., Moll, T., Auer, H. and Nasmyth, K. (1992) A central role for SWI6 in modulating cell cycle Start-specific transcription in yeast. *Nature*, **357**, 508-13.

Dollard, C., Ricupero-Hovasse, S.L., Natsoulis, G., Boeke, J.D. and Winston, F. (1994) SPT10 and SPT21 are required for transcription of particular histone genes in Saccharomyces cerevisiae. *Mol Cell Biol*, **14**, 5223-8.

Drapkin, B.J., Lu, Y., Procko, A.L., Timney, B.L. and Cross, F.R. (2009) Analysis of the mitotic exit control using locked levels of stable mitotic cyclin. *Mol Syst Biol*, **5**:328.

Eisen, M.B., Spellman, P.T., Brown, P.O. and Botstein, D. (1998) Cluster analysis and display of genome-wide expression patterns. *Proc Natl Acad Sci U S A*, **95**, 14863-8.

Eldar, A., Chary, V.K., Xenopoulos, P., Fontes, M.E., Loson, O.C., Dworkin, J., Piggot, P.J. and Elowitz, M.B. (2009) Partial penetrance facilitates developmental evolution in bacteria. *Nature*, **460**, 510-4.

Elowitz, M.B., Levine, A.J., Siggia, E.D. and Swain, P.S. (2002) Stochastic gene expression in a single cell. *Science*, **297**, 1183-6

Enquist-Newman, M., Sullivan, M. and Morgan, D.O. (2008) Modulation of the mitotic regulatory network by APC-dependent destruction of the Cdh1 inhibitor Acm1. *Mol Cell*, **30**, 437-46.

Epstein, C.B. and Cross, F.R. (1992) CLB5: a novel B cyclin from budding yeast with a role in S phase. *Genes Dev*, **6**, 1695-1706.

Eser, U., Falleur-Fettig, M., Johnson, A. and Skotheim, J.M. (2011) Commitment to a cellular transition precedes genome-wide transcriptional change. *Mol Cell*, **43**, 515-27.

Ferrezuelo, F., Colomina, N., Futcher, B. and Aldea, M. (2010) The transcriptional network activated by Cln3 cyclin at the G1-to-S transition of the yeast cell cycle. *Genome Biol*, **11**:R67.

Gourguechon, S., Holt, L.J., Cande, W.Z. (2013) The Giardia cell cycle progresses independently of the anaphase-promoting complex. *J Cell Sci*, **126**, 2246-55.

Hall, M.C., Warren, E.N. and Borchers, C.H. (2004) Multi-kinase phosphorylation of the APC/C activator Cdh1 revealed by mass spectrometry. *Cell Cycle*, **3**, 1278-1284.

Hao, B., Oehlmann, S., Sowa, M.E., Harper, J.W., and Pavletich, N.P. (2007) Structure of a Fbw7-Skp1-cyclin E complex: multisite-phosphorylated substrate recognition by SCF ubiquitin ligases. *Mol Cell*, **26**, 131-43.

Hildebrandt, E.R. and Hoyt, M.A. (2001) Cell cycle-dependent degradation of the Saccharomyces cerevisiae spindle motor Cin8p requires APC(Cdh1) and a bipartite destruction sequence. *Mol Biol Cell*, **12**, 3402-3416.

Holt, L.J., Tuch, B.B., Villen, J., Johnson, A.D., Gygi, S.P. and Morgan, D.O. (2009) Global analysis of Cdk1 substrate phosphorylation sites provides insights into evolution. *Science*, **325**, 1682-1686.

Huang, J.N., Park, I., Ellingson, E., Littlepage, L.E. and Pellman, D. (2001) Activity of the APC(Cdh1) form of the anaphase-promoting complex persists until S phase and prevents the premature expression of Cdc20p. *J Cell Biol*, **154**, 85-94.

Jaquenoud, M., van Drogen, F. and Peter, M. (2002) Cell cycle-dependent nuclear export of Cdh1p may contribute to the inactivation of APC/C(Cdh1). *EMBO J*, **21**, 6515-6526.

Juang, Y.L., Huang, J., Peters, J.M., McLaughlin, M.E., Tai, C.Y. and Pellman, D. (1997) APC-mediated proteolysis of Ase1 and the morphogenesis of the mitotic spindle. *Science*, **275**, 1311-4.

Kim, S.Y. and Ferrell, J.E., Jr. (2007) Substrate competition as a source of ultrasensitivity in the inactivation of Wee1. *Cell,* **128**, 1133-1145.

King, R.W., Peters, J.M., Tugendreich, S., Rolfe, M., Hieter, P. and Kirschner, M.W. (1995) A 20S complex containing CDC27 and CDC16 catalyzes the mitosis-specific conjugation of ubiquitin to cyclin B. *Cell*, **81**, 279-288.

Knapp, D., Bhoite, L., Stillman, D.J. and Nasmyth, K. (1996) The transcription factor Swi5 regulates expression of the cyclin kinase inhibitor p40SIC1. *Mol Cell Biol*, **16**, 5701-7.

Koivomagi, M., Valk, E., Venta, R., Iofik, A., Lepiku, M., Balog, E.R., Rubin, S.M., Morgan, D.O. and Loog, M. (2011) Cascades of multisite phosphorylation control Sic1 destruction at the onset of S phase. *Nature*, **480**, 128-31.

Komeili, A. and O'Shea, E.K. (1999) Roles of phosphorylation sites in regulating activity of the transcription factor Pho4. *Science*, **284**, 977-980.

Koranda, M., Schleiffer, A., Endler, L. and Ammerer, G. (2000) Forkhead-like transcription factors recruit Ndd1 to the chromatin of G2/M-specific promoters. *Nature*, **406**, 94-8.

Kussell, E. and Leibler, S. (2005) Phenotypic diversity, population growth, and information in fluctuating environments. *Science*, **309**, 2075-8.

Levy, S.F., Ziv, N. and Siegal, M.L. (2012) Bet hedging in yeast by

heterologous, age-correlated expression of a stress protectant. *PLoS Biol*, **10**:e1001325.

Lew, D.J. and Reed, S.I. (1993) Morphogenesis in the yeast cell cycle: regulation of Cdc28 and cyclins. *J Cell Biol*, **120**, 1305-20.

Loog, M. and Morgan, D.O. (2005) Cyclin specificity in the phosphorylation of cyclin-dependent kinase substrates. *Nature*, **434**, 104-8.

Lord, P.G. and Wheals, A.E. (1981) Variability in individual cell cycles in Saccharomyces cerevisiae. *J Cell Sci*, **50**, 361-76.

Lu, Y. and Cross, F.R. (2010) Periodic cyclin-Cdk activity entrains an autonomous Cdc14 release oscillator. *Cell*, **141**, 268-79

Maamar, H., Raj, A. and Dubnau, D. (2007) Noise in gene expression determines cell fate in Bacillus subtilis. *Science*, **317**, 526-9.

Martinez, J.S., Jeong, D.E., Choi, E., Billings, B.M. and Hall, M.C. (2006) Acm1 is a negative regulator of the CDH1-dependent anaphase-promoting complex/cyclosome in budding yeast. *Mol Cell Biol*, **26**, 9162-9176.

Melesse, M., Choi, E., Hall, H., Walsh, M.J., Geer, M.A. and Hall, M.C. (2014) Timely activation of budding yeast APCCdh1 involves degradation of its inhibitor, Acm1, by an unconventional proteolytic mechanism. *PLoS One*, **9**, e103517.

Milloz, J., Duveau, F., Nuez, I. and Felix, M.A. (2008) Intraspecific evolution of the intercellular signaling network underlying a robust developmental system. *Genes Dev*, **22**,3064-75.

Morgan, D.O. (2007) The cell cycle: principles of control. *New Science Press, London*

Murray, A.W. (2004) Recycling the cell cycle: cyclins revisited. *Cell*, **116**, 221-34.

Nash, P., Tang, X., Orlicky, S., Chen, Q., Gertler, F.B., Mendenhall, M.D., Sicheri, F., Pawson, T. and Tyers, M. (2001) Multisite phosphorylation of a CDK inhibitor sets a threshold for the onset of DNA replication. *Nature*, **414**, 514-521.

Newman, J.R., Ghaemmaghami, S., Ihmels, J., Breslow, D.K., Noble, M., DeRisi, J.L. and Weissman, J.S. (2006) Single-cell proteomic analysis of S. cerevisiae reveals the architecture of biological noise. *Nature*, **441**, 840-6.

Orlando, D.A., Lin, C.Y., Bernard, A., Wang, J.Y., Socolar, J.E., Iversen, E.S., Hartemink, A.J. and Haase, S.B. (2008) Global control of cell-cycle transcription by coupled CDK and network oscillators. *Nature*, **453**, 944-7.

Pramila, T., Wu, W., Miles, S., Noble, W.S. and Breeden, L.L. (2006) The Forkhead transcription factor Hcm1 regulates chromosome segregation genes and fills the S-phase gap in the transcriptonal circuitry of the cell cycle. *Genes Dev*, **20**, 2266-78.

Rahi, S.J., Ondracka, A., Pecani, K., Oikonomou, C. and Cross, F.R. Entrainment of periodic trascription to the CDK/APC oscillator. *Manuscript submitted*

Richardson, H., Lew, D.J., Henze, M., Sugimoto, K. and Reed, S.I. (1992) Cyclin-B homologs in Saccharomyces cerevisiae function in S phase and in G2. *Genes Dev*, **6**, 2021-34.

Richardson, H.E., Wittenberg, C., Cross, F.R., and Reed, S.I. An essential G1 function for cyclin-like proteins in yeast. Cell, **59**, 1277-33

Robbins, J.A., and Cross, F.R. (2010a) Requirements and reasons for effective inhibition of the anaphase promoting complex activator CDH1. *Mol Biol Cell*, **21**, 914-25.

Robbins, J.A., and Cross, F.R. (2010b) Regulated degradation of the APC coactivator Cdc20. *Cell Div*, **5**:23.

Robbins, Jonathan. PhD Thesis. The Rockefeller University, 2010.

Rudner, A.D. and Murray, A.W. (2000) Phosphorylation by Cdc28 activates the Cdc20-dependent activity of the anaphase-promoting complex. *J Cell Biol*, **149**, 1377-1390.

Schneider, B.L., Patton, E.E., Lanker, S., Mendenhall, M.D., Wittenberg, C., Futcher, B. and Tyers, M. (1998) Yeast G1 cyclins are unstable in G1 phase. *Nature*, **395**, 86-89.

Schreiber, A., Stengel, F., Zhang, Z., Enchev, R.I., Kong, E.H., Morris, E.P., Robinson, C.V., da Fonseca, P.C. and Barford, D. (2011) Structural basis for the subunit assembly of the anaphase-promoting complex. *Nature*, **470**, 227-32.

Schwab, M., Lutum, A.S. and Seufert, W. (1997) Yeast Hct1 is a regulator of Clb2 cyclin proteolysis. *Cell*, **90**, 683-693.

Schwob, E. and Nasmyth, K. (1993) CLB5 and CLB6, a new pair of B cyclins involved in DNA replication in Saccharomyces cerevisiae. *Genes Dev*, **7**, 1160-1175.

Schwob, E., Bohm, T., Mendenhall, M.D. and Nasmyth, K. (1994) The B-type cyclin kinase inhibitor p40SIC1 controls the G1 to S transition in S. cerevisiae. *Cell*, **79**, 233-44.

Shirayama, M., Toth, A., Galova, M. and Nasmyth, K. (1999) APC(Cdc20) promotes exit from mitosis by destroying the anaphase inhibitor Pds1 and cyclin Clb5. *Nature*, **402**, 203-207.

Sia, R.A., Herald, H.A. and Lew, D.J. (1996) Cdc28 tyrosine phosphorylation and the morphogenesis checkpoint in budding yeast. *Mol Biol Cell*, **7**, 1657-66.

Simmons-Kovacs, L.A., Mayhew, M.B., Orlando, D.A., Jin, Y., Li, Q., Huang, C., Reed, S.I., Mukherjee, S. and Haase, S.B. (2012) Cyclin-dependent kinases are regulators and effectors of oscillations driven by a transcription factor network. *Mol Cell*, **45**, 669-79.

Skotheim, J.M., Di Talia, S., Siggia, E.D. and Cross, F.R. (2008) Positive feedback of G1 cyclins ensures coherent cell cycle entry. *Nature*, **454**, 291-296.

Spellman, P.T., Sherlock, G., Zhang, M.Q., Iyer, V.R., Anders, K., Eisen, M.B., Brown, P.O., Botstein, D. and Futcher, B. (1998) Comprehensive identification of cell cycle-regulated genes of the yeast Saccharomyces cerevisiae by microarray hybridization. *Mol Biol Cell*, **9**, 3273-3297.

Strickfaden, S.C., Winters, M.J., Ben-Ari, G., Lamson, R.E., Tyers, M. and Pryciak, P.M. (2007) A mechanism for cell-cycle regulation of MAP kinase signaling in a yeast differentiation pathway. *Cell*, **128**, 519-531.

Sudakin, V., Ganoth, D., Dahan, A., Heller, H., Hershko, J., Luca, F.C., Ruderman, J.V. and Hershko, A. (1995) The cyclosome, a large complex containing cyclin-selective ubiquitin ligase activity, targets cyclins for destruction at the end of mitosis. *Mol Biol Cell*, **6**, 185-197.

Tulin, F., and Cross, F.R. Environmental cues and cyclin-dependent kinases control diurnal transcription in Chlamydomonas. *Manuscript submitted*

Tyers, M. (1996) The cyclin-dependent kinase inhibitor p40SIC1 imposes the requirement for Cln G1 cyclin function at Start. *Proc Natl Acad Sci U S A*, **93**, 7772-6.

Visintin, R., Prinz, S. and Amon, A. (1997) CDC20 and CDH1: a family of substrate-specific activators of APC-dependent proteolysis. *Science*, **278**, 460-3.

Visintin, R., Hwang, E.S. and Amon, A. (1999) Cfi1 prevents premature exit from mitosis by anchoring Cdc14 phosphatase in the nucleolus. *Nature*, **398**, 818-23.

Wang, H., Carey, L.B., Cai, Y., Wijnen, H., and Futcher, B. Recruitment of Cln3 cyclin to promoters controls cell cycle entry via histone deacetylase and other targets. *PLoS Biology*, **7**, e1000189.

Wasch, R. and Cross, F.R. (2002) APC-dependent proteolysis of the mitotic cyclin Clb2 is essential for mitotic exit. *Nature*, **418**, 556-62.

Yeong, F.M., Lim, H.H., Wang, Y. and Surana, U. (2001) Early expressed Clb proteins allow accumulation of mitotic cyclin by inactivating proteolytic machinery during S phase. *Mol Cell Biol*, **21**, 5071-5081.

Zachariae, W., Schwab, M., Nasmyth, K. and Seufert, W. (1998) Control of cyclin ubiquitination by CDK-regulated binding of Hct1 to the anaphase promoting complex. *Science*, **282**, 1721-1724.

Zenklusen, D., Larson, D.R. and Singer, R.H. (2008) Single-RNA counting reveals alternative modes of gene expression in yeast. *Nat Struct Mol Biol*, **15**, 1263-71.